

A Unique Case of Oxidative Addition of Interhalogens IX (X = Cl, Br) to Organodiselenone Ligands: Nature of the Chemical Bonding in Asymmetric I–Se–X Polarised Hypervalent Systems

Emilio José Juárez-Pérez,^[a] M. Carla Aragoni,^[b] Massimiliano Arca,^[b]
Alexander J. Blake,^[c] Francesco A. Devillanova,^[b] Alessandra Garau,^[b]
Francesco Isaia,^[b] Vito Lippolis,^{*,[b]} Rosario Núñez,^[a] Anna Pintus,^[b] and Claire Wilson^[c]

Abstract: The reactivity of the imidazoline-2-selone derivatives 1,1'-methylenebis(3-methyl-4-imidazoline-2-selone) (**D1**) and 1,2-ethylenebis(3-methyl-4-imidazoline-2-selone) (**D2**) towards the interhalogens IBr and ICl has been investigated in the solid state with the aim of synthesising “T-shaped” hypervalent chalcogen compounds featuring the extremely rare linear asymmetric I–E–X moieties (E = S, Se; X = Br, Cl). X-ray diffraction analysis and FT-Raman measurements provided a clear indication of the presence in the compounds ob-

tained of discrete molecular adducts containing I–Se–Br and I–Se–Cl hypervalent moieties following a unique oxidative addition of interhalogens IX (X = Cl, Br) to the organoselone ligands. In all asymmetric hypervalent systems isolated, a strong polarisation was observed, with longer bond lengths at the selenium atom involving the

most electronegative halogen. A topological electron density analysis on model compounds based on the quantum theory of atoms-in-molecules (QTAIM) and electron localisation function (ELF) established the three-centre–four-electron (3c–4e) nature of the bonding in these very polarised selenium hypervalent systems and new criteria were suggested to define and ascertain the hypervalency of the selenium atoms in these and related halogen and interhalogen adducts.

Keywords: charge transfer • density functional calculations • halogens • hypervalent compounds • oxidative addition • selenium

Introduction

It is well known that chalcogen(II) halides (EX₂; E = S, Se, Te; X = F, Cl, Br, I) are generally unstable under ambient experimental conditions and therefore their chemistry has not been widely studied. However, it is also known that they can be stabilised as adducts of Lewis bases.^[1] The most common synthetic approach to such adducts is the reduction of chalcogen(IV) halides or organohalides in the presence of electron-pair donors that may also act as reducing agents.^[2] An alternative synthetic method involves the oxidative addition of dihalogens, X₂, to chalcogen-containing

donor molecules.^[3,4] For example, the addition of Cl₂ to 1,3-dimethylimidazoline-2-thione^[5] and of Br₂ to 1,3-dimethylimidazoline-2-selone^[6] affords stable compounds featuring linear Cl–S–Cl and Br–Se–Br groups, respectively, that are perpendicular to the imidazoline ring. These products can also be formally regarded as adducts between 1,3-dimethylimidazoline-2-ylidene and SCl₂ or SeBr₂.^[7–9] Adducts of this kind are commonly referred to as “T-shaped” hypervalent chalcogen compounds featuring a linear X–E–X moiety (X = Cl, Br, I). With donors of the type R₂C=E (E = S, Se), the “T-shaped” nature of the corresponding adducts derived from the oxidative addition of a molecule of X₂ to the chalcogen atom is well explained by the VSEPR model,^[10] according to which the geometry at the chalcogen atom is pseudo-trigonal-bipyramidal (tbp) with the halogen atoms occupying the apical positions (two lone pairs and one bonding pair in the plane perpendicular to the X–E–X direction). The geometry is disphenoidal in the case of R₂E donor molecules (one lone pair and two bond pairs in the plane perpendicular to the X–E–X direction). These compounds are also commonly reported as 10–E–3 (R₂C=E donors) or 10–E–4 (R₂E donors) hypervalent systems, which indicates that the chalcogen atom, E, is formally associated with five electron pairs (10 electrons), only three or four of which, respectively, are bond pairs.^[7,11,12] As for trihalides, X₃[–], the chemical bond in the linear X–E–X fragment can be described by using the 3c–4e bonding scheme, the simpli-

[a] Dr. E. J. Juárez-Pérez, Dr. R. Núñez
Institut de Ciència de Materials de Barcelona (ICMAB-CSIC)
Campus UAB
08193 Bellaterra, Barcelona (Spain)

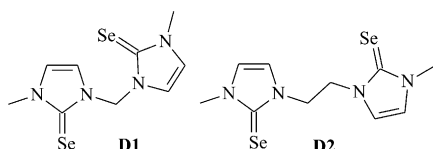
[b] Dr. M. C. Aragoni, Dr. M. Arca, Prof. F. A. Devillanova,
Dr. A. Garau, Prof. F. Isaia, Prof. Dr. V. Lippolis, Dr. A. Pintus
Dipartimento di Chimica Inorganica ed Analitica
S.S. 554 Bivio per Sestu
Università degli Studi di Cagliari, I-09042 Monserrato, CA (Italy)
Fax.: (+39)070-675-4456
E-mail: lippolis@unica.it

[c] Prof. Dr. A. J. Blake, Dr. C. Wilson
School of Chemistry, The University of Nottingham
University Park, Nottingham, NG7 2RD (UK)

Supporting information for this article is available on the WWW under <http://dx.doi.org/10.1002/chem.201100970>.

fied MO diagram of which can be constructed by combining the p_z atomic orbitals of the central chalcogen and those of the two terminal halogen atoms: four electrons occupy the bonding and non-bonding orbitals, thus conferring a total bond order of 1 (0.5 for each E–X bond).^[11,13] This description agrees with the observation that the experimental E–X bond lengths in X–E–X fragments are about 10% longer than normal single chalcogen–halogen bonds. Furthermore, on decreasing the electronegativity difference between the halogen and the chalcogen, starting from the reaction between chalcogen donors, in particular donor molecules containing the $>C=E$ (E=S, Se) groups, and dihalogens, X_2 , charge-transfer (CT) adducts bearing the linear E–X–X group are formed in preference to “T-shaped” adducts. In fact, no “T-shaped” sulfur adducts with I_2 have so far been reported, whereas three with Br_2 have been structurally characterised.^[5,14] On the other hand, analogous selenium adducts with Br_2 are numerous,^[13,15] whereas only three examples with I_2 have been reported.^[16] Hypervalent sulfur and selenium compounds containing the linear Cl–E–Cl (E=S, Se) group are very well known.^[13,15] In principle, hypervalent chalcogen compounds should also be isolable from the reactions of chalcogen donors with interhalogens IX (X=Cl, Br), but in fact, after the first compound bearing the linear I–Se–Br group that we prepared from **D2** (Scheme 1) following this very synthetic procedure,^[17] no further “T-shaped” adducts featuring I–E–X (E=S, Se; X=Cl, Br) moieties have been characterised, which indicates a very low tendency of interhalogens to undergo oxidative addition to chalcogen donor atoms and in particular to chalcogen carbonyl $>C=E$ groups. As proved in the only case known of oxidative addition of IBr to a selone group,^[17] “T-shaped” adducts featuring I–E–X (E=S, Se; X=Cl, Br) moieties should in principle be characterised by a strong polarisation of the E–X bond, thereby establishing appreciable ionic character in this bond with the chalcogen atom still remaining in a hypervalent state and the E–I bond order moving from 0.5 towards 1.^[17]

Through this paper we contribute to this area of chemistry by reporting a complete survey of the reactivity of imidazoline-2-selone derivatives **D1** and **D2** (Scheme 1) towards IBr and ICl. Unprecedented oxidative addition products have been isolated in which chalcogen...halogen soft-soft interactions contribute to the self-assembly of interesting supramolecular structures. X-ray diffraction analysis, FT-Raman spectroscopy and DFT QTAIM studies were used to determine the nature of both the overall structures of the compounds isolated and the chemical bonding in I–Se–X (X=Cl, Br) and related moieties.



Scheme 1.

Results and Discussion

Synthesis and X-ray diffraction analysis: It is well known that the reaction of dihalogens, X_2 , with donor molecules containing the $>C=E$ (E=S, Se) group can afford a great variety of products (i.e., CT and “T-shaped” adducts, $[>C-E-E-C<]^{2+}$ dicationic species and $[>C-E-X-E-C<]^+$ and $[>C-E-X]^+$ cations) with different structural archetypes depending on both the acid/base nature of the reactants and the experimental conditions used.^[14–21] The goal of this work was to gain an understanding not only of the chemical bond in the species formed,^[13] but also of the possible pathways that allow the interconversion between the various species in equilibrium.^[14b,22,23] For this, a wide survey of the reactivity of different chalcogenone donors featuring $>C=E$ (E=S, Se) groups towards dihalogens and interhalogens under different experimental conditions is necessary.

Some years ago we studied the reactivity of imidazoline-2-selone derivatives **D1** and **D2** (Scheme 1) towards I_2 and Br_2 .^[6b,16a] Hypervalent 10–Se–3 “T-shaped” compounds bearing Br–Se–Br groups were isolated from the reactions of these two selenium donors with Br_2 . Structurally analogous I_2 adducts were isolated only in the case of **D2**, whereas a CT adduct featuring a Se–I–I group was obtained in the case of **D1**. We moved on, therefore, to consider the reactivity of **D1** and **D2** towards interhalogens IX (X=Cl, Br) in the hope of isolating hypervalent oxidative addition products bearing I–Se–X moieties.^[17]

From the reaction of IBr with **D2** in a 2:1 molar ratio in CH_3CN , we isolated the compound **D2**·2IBr (**III**), which represents the first and so far only example of a “T-shaped” I–Se–Br adduct.^[17] In **III** the general structural features of the two I–Se–Br groups are not very different from those found for the I–Se–I and Br–Se–Br groups in the “T-shaped” adducts of **D2** with I_2 and Br_2 , respectively^[6b,16a] (they are approximately linear and perpendicular to the associated organic penta-atomic ring, see the Supporting Information), with the important difference that in **III** the Se–I bonds are significantly shorter than the Se–Br bonds. DFT calculations in the gas phase indicated a more ionic character for the Se–Br bond compared with the Se–I bond and supported for each linear I–Se–Br group in **III** a bonding situation intermediate between a pure covalent 3c–4e system and an I–Se⁺...Br[–] ionic couple, the chalcogen atom, therefore, still being in a hypervalent state.^[17] Intramolecular hydrogen bonds involving bromine atoms and soft-soft I...Br contacts between two symmetry-related units of **III** to form dimeric assemblies (see the Supporting Information) certainly contribute in the solid state to a further polarisation of the Se–Br bond in the I–Se–Br systems of **III** in such a way as to reverse, at the end, the order of the Se–Br and Se–I bond lengths that would be predicted on the basis of the atomic radii of the species involved and that is calculated in the gas phase [$d(Se-Br) < d(Se-I)$].^[17]

The reactions of **D1** with IBr in molar ratios of 1:2 and 1:4 in CH_3CN afforded compounds **I** and **II**, respectively, which gave slightly different elemental analysis results. X-

ray diffraction analysis confirmed in both cases the formation of “T-shaped” hypervalent adducts at both chalcogen sites of the donor. In each case, during the structure refinement using a Br–Se–Br model for the two hypervalent moieties in the asymmetric unit, an anomalous displacement parameter for one of the bromine sites in both hypervalent moieties suggested that these bromine sites might be partially replaced by iodine. The refinement of the disordered models, in which the simultaneous presence of these two halogens in the same site was considered, gave the best fitting to the data with I/Br occupancies of 0.42/0.58 and 0.67/0.33 for sites 1 and 4, respectively, in **I** (Figure 1) and 0.53/0.47 and 0.17/0.83 for sites 1 and 4, respectively, in **II** (see the Supporting Information).

Therefore, compounds **I** and **II** must be formulated as **D1**·Br_{2.91}I_{1.09} and **D1**·Br_{3.30}I_{0.70}, respectively, in good agreement with the microanalytical data. Because the electron density corresponding to the hypervalent systems in **I** and **II** is an average of the contents of all unit cells in the crystals, the fitting of the data with mixed I/Br occupancies is unable to give a clear indication of the presence in the crystals of **I** and **II** of discrete molecular adducts containing the I–Se–Br or Br–Se–Br hypervalent moieties. In both compounds the Br–Se–X (X=I/Br) hypervalent moieties are almost linear [Br–Se–X ranging from 172.97(5) to 176.50(5)°] and roughly perpendicular to the average plane of the imidazolidine moiety [N(1/3)–C(1/6)–Se(1/2)–X ranging from 77.2(8) to 87.2(9)° (absolute values)]. As reported for **D2**·2IbR (**III**),^[17] in both **I** and **II** the Se–Br distances are longer than those of Se–X (X=I/Br). The conformations of the adduct molecules are determined by two weak intramolecular hydrogen-bonding interactions (shown as dotted lines in Figure 1),

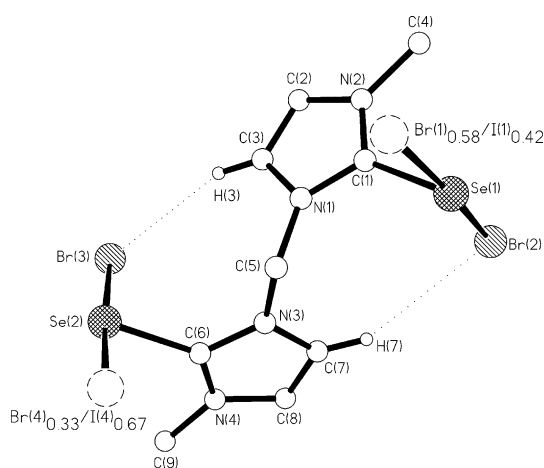


Figure 1. View of **I** showing the numbering scheme adopted. For clarity only those hydrogen atoms involved in intramolecular hydrogen bonds (dotted lines) are shown. Bond lengths [Å] and angles [°]: C(1)–Se(1) 1.883(10), Se(1)–X(1) 2.593(3), Se(1)–Br(2) 2.673(3), C(6)–Se(2) 1.893(10), Se(2)–Br(3) 2.739(2), Se(2)–X(4) 2.627(2), C(1)–Se(1)–X(1) 90.1(3), C(1)–Se(1)–Br(2) 83.4(3), C(6)–Se(2)–Br(3) 84.2(3), C(6)–Se(2)–X(4) 94.3(3), X(1)–Se(1)–Br(2) 173.46(5), Br(3)–Se(2)–X(4) 176.50(5); Br(2)···H(7) 2.95, Br(2)–C(7) 3.836(10), C(7)–H(7)–Br(2) 155; Br(3)···H(3) 2.99, Br(3)–C(3) 3.904(11), C(3)–H(3)–Br(3) 161 [X(1) = Br(1)_{0.58}/I(1)_{0.42}, X(4) = Br(4)_{0.33}/I(4)_{0.67}].

each one involving the site fully occupied by the bromine of the hypervalent moieties. These bromine atoms are also involved in an intricate network of intermolecular hydrogen-bonding interactions. On the other hand, in both compounds (see Figure 2 for **I** and Supporting Information for **II**), only

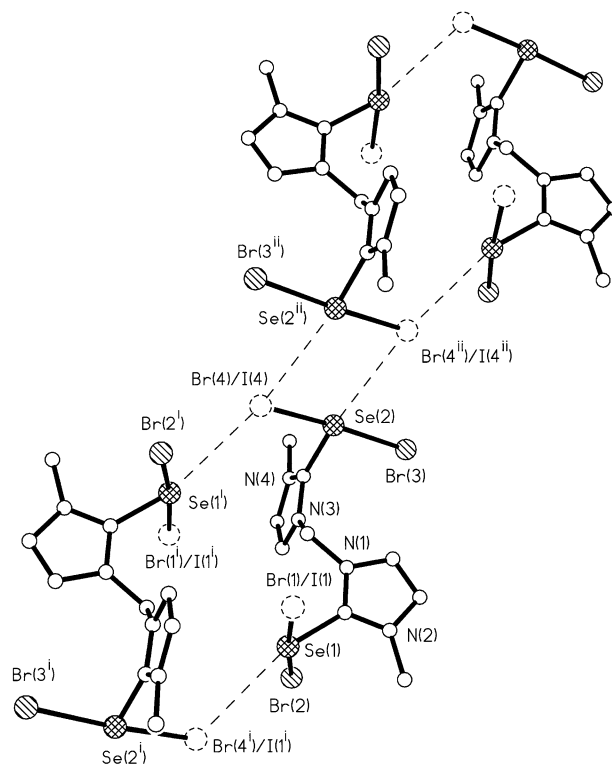


Figure 2. Partial view of the crystal packing in **I** showing the selenium···halogen contacts (dashed lines). Bond lengths [Å] and angles [°]: Se(1)···X(4) 3.576(2), Se(2)···X(4) 3.610(3), Se(1)–X(4)–Se(2) 141.48(5), Se(2)–X(4)–Se(1) 123.97(6), Se(2)–X(4)–Se(2) 86.34(7), X(4)–Se(2)–X(4) 93.66(7) [X(4) = Br(4)_{0.33}/I(4)_{0.67}]. Symmetry codes: i = –x, –y, –z; ii = 1–x, –y–1, –z.

one of the two mixed occupied I/Br sites is involved in two intermolecular Se···X contacts with two symmetry-related adduct units, with distances ranging from 3.564(2) to 3.610(3) Å. In this way, chain-like supramolecular arrays of adduct molecules of **I** or **II** are formed by different types of “T–T” associations between the “T-shaped” hypervalent moieties and involving I/Br-bridging soft–soft interactions, each selenium atom resulting in a square planar 14–Se–4 hypervalent environment.^[24] The products **I** and **II** isolated from the reactions of **D1** with IBr in different molar ratios in CH₃CN clearly illustrate an additional complication through the possibility of obtaining a “T-shaped” I–E–X (X=Br, Cl) adduct by direct reaction of chalcogenone donor molecules with IX (X=Cl, Br) interhalogens by oxidative addition, that is, the tendency of interhalogens to disproportionate giving rise to I₂ and X₂ molecules.^[23b,25]

The great importance of the experimental conditions and the nature of the reactants in determining the outcome of the reactions between dihalogens or interhalogens and

donor molecules containing the $>C=E$ ($E=S, Se$) group is also proved in the case of the reaction of **D1** or **D2** with IBr. In fact, by using a 1:4 molar ratio of **D2**/IBr, a $[D2]^{2+}$ dication featuring an intramolecular Se–Se bond and balanced by two linear trihalides [a symmetric IX_2^- ($X=I_{0.30}/Br_{0.70}$) located in a special position and an asymmetric $BrIX^-$ ($X=I_{0.47}/Br_{0.53}$), both with mixed occupied halogen sites] was isolated from CH_3CN (compound **IV**, see Figure 3). Both selenium atoms in the cyclic $[D2]^{2+}$ dication are involved in soft–soft $Se\cdots X$ interactions with the coun-

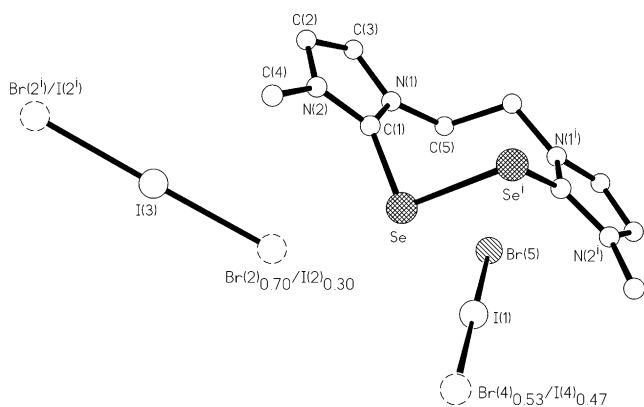


Figure 3. View of **IV** showing the numbering scheme adopted. Bond lengths [\AA] and angles [$^\circ$]: C(1)–Se 1.894(7), Se–Seⁱ 2.3602(14), I(1)–Br(5) 2.7539(13), I(1)–X(4) 2.7768(12), I(3)–X(2) 2.7752(10), C(1)–Se–Seⁱ 97.64(19), Br(5)–I(1)–X(4) 180.0, X(2)–I(3)–X(2) 178.49(4) [X(2) = Br(2)_{0.70}/I(2)_{0.30}, X(4) = Br(4)_{0.53}/I(4)_{0.47}]. Symmetry code: $i = -x, y, -1/2 - z$.

ter-anions to form continuous undulating two-dimensional layers (Figure 4). Each layer consists of sinusoidal polymeric successions of alternating head-to-tail interacting dications and IX_2^- units [$Se\cdots X$ 3.396(1) \AA] cross-linked by the $BrIX^-$ units through $Se\cdots X$ bridging interactions [$Se\cdots X$ 3.711(2) \AA ; Figure 4].

Many authors have attempted to judge whether the different products obtainable from the reactions of chalcogenone donor molecules [$>C=E$ ($E=S, Se$)] with halogens or interhalogens would originate from a common intermediate species. In particular, Husebye proposed that this species would be the $[>C-E-X]^+$ cation ($E=S, Se; X=I, Br$), which can undergo attack from an appropriate nucleophile either on the chalcogen or halogen site.^[22] If the nucleophilic species is a chalcogenone donor, both a $[>C-E-E-C<]^{2+}$ dication and a $[>C-E-X-E-C<]^+$ monocation can be formed. In the case of X^- as nucleophilic species, CT and “T-shaped” hypervalent adducts are possible as products.^[22] Whether this cation really forms in solution has not been proved in all cases considered, but it has been observed that the charge distribution calculated on $[>C-E-X]^+$ can be of great help in predicting the nature of the final products.^[14b,23b]

With the aim of synthesising the first example of a “T-shaped” I–Se–Cl hypervalent adduct by oxidative addition of ICl to chalcogenone donor molecules, we treated **D1** and **D2** with ICl under different experimental conditions. The reactions of **D1** with ICl in a molar ratio of 1:4 in CH_3CN gave compound **V**, which yields microanalytical data slightly different from those expected for the formulation **D1**·Cl₄·X-

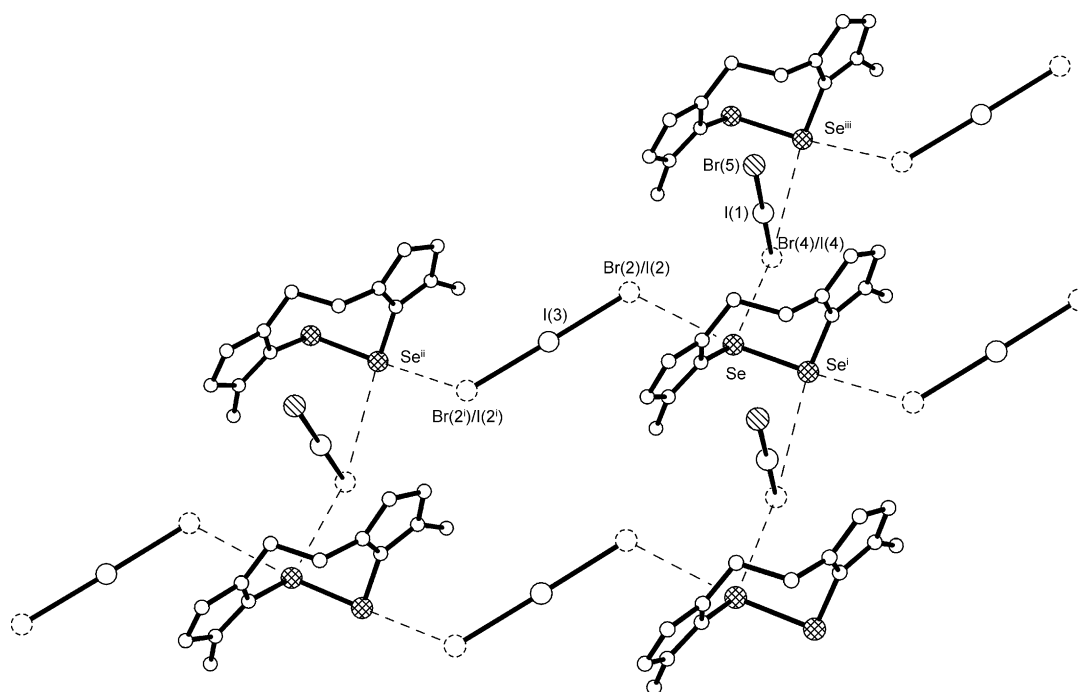


Figure 4. Partial view of the crystal packing in **IV** showing the selenium...halogen contacts (dashed lines). Bond lengths [\AA] and angles [$^\circ$]: $Se\cdots X(4)$ 3.711(2), $Se\cdots X(2)$ 3.396(1), $Se^{ii}\cdots X(4)$ 3.711(2), $Se^{ii}\cdots X(2)$ 3.396(1), $Se-X(2)-I(3)$ 120.38(3), $Se-X(4)-Se^{iii}$ 145.13(4) [X(2) = Br(2)_{0.70}/I(2)_{0.30}, X(4) = Br(4)_{0.53}/I(4)_{0.47}]. Symmetry codes: $i = -x, y, -1/2 - z$; $ii = -x, y, 1/2 - z$; $iii = -1 + x, y, -1/2 - z$.

ray diffraction analysis confirmed the formation of a “T-shaped” hypervalent adduct featuring a Cl–Se–Cl moiety at one chalcogen site of the donor molecule and a Cl–Se–X (X = Cl_{0.86}/I_{0.14}) moiety at the other chalcogen site (Figure 5),

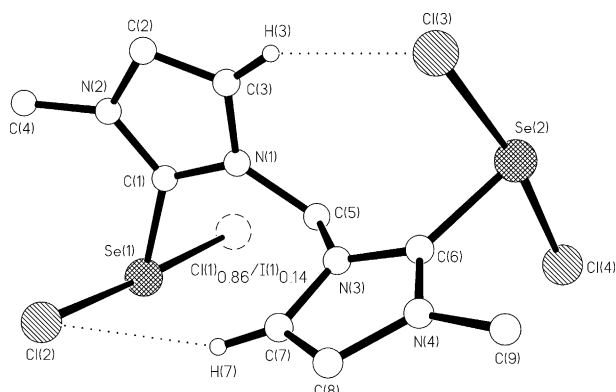


Figure 5. View of **V** showing the numbering scheme adopted. For clarity only those hydrogen atoms involved in intramolecular hydrogen bonds (dotted lines) are shown. Bond lengths [Å] and angles [°]: C(1)–Se(1) 1.882(5), Se(1)–X(1) 2.425(2), Se(1)–Cl(2) 2.548(2), C(6)–Se(2) 1.881(6), Se(2)–Cl(3) 2.473(2), Se(2)–Cl(4) 2.361(2), C(1)–Se(1)–X(1) 92.01(18), C(1)–Se(1)–Cl(2) 82.96(18), Cl(2)–Se(1)–X(1) 174.76(5), C(6)–Se(2)–Cl(3) 82.87(18), C(6)–Se(2)–Cl(4) 88.51(18), Cl(4)–Se(2)–Cl(3) 171.55(6); Cl(2)···H(7) 2.89, Cl(2)–C(7) 3.784(5), C(7)–H(7)–Cl(2) 156; Cl(3)···H(3) 2.90, Cl(3)–C(3) 3.769(6), C(3)–H(3)–Cl(3) 153 [X(1) = C(1)_{0.86}/I(1)_{0.14}].

in agreement with a similar or even higher tendency of ICl to disproportionate in comparison with IBr. Both hypervalent groups in **V** are asymmetric as a result of the polarisation determined by weak intramolecular hydrogen-bonding interactions similar to those observed in **I–III** (see Figures 1 and 5) and the mixed I/Cl occupancy observed at one halogen site in one of the two hypervalent moieties (see the discussion above). Interestingly, within the same molecule of adduct **V**, the overall length of the Cl–Se–X (X = Cl/I) group is longer than the corresponding distance in the Cl–Se–Cl fragment (Figure 5), with the Se–X bond length shorter than the Se–Cl distance within the Cl–Se–X group, analogously to what was observed for the I–Se–X (X = Br/I) groups in **I–III**. “T–T” associations between the “T-shaped” hypervalent moieties of different units of **V**, and involving I/Cl-bridging Se···X soft–soft interactions, give rise to chain-like supramolecular assemblies in the crystal lattice similar to those observed in the cases of **I** and **II** (see the Supporting Information).

Two different compounds, forming as orange and black crystals were obtained from a CH₃CN solution of **D2** and ICl (molar ratio of 1:4) after slow evaporation of the solvent at room temperature. X-ray diffraction analysis of both types of crystals was undertaken to ascertain their nature. The orange crystals, which are the minor reaction product, were found by crystallographic analysis to be the adduct **D2**·Cl₄ (**VI**); this features two almost linear “T-shaped” Cl–Se–Cl hypervalent moieties (Figure 6). The two hypervalent

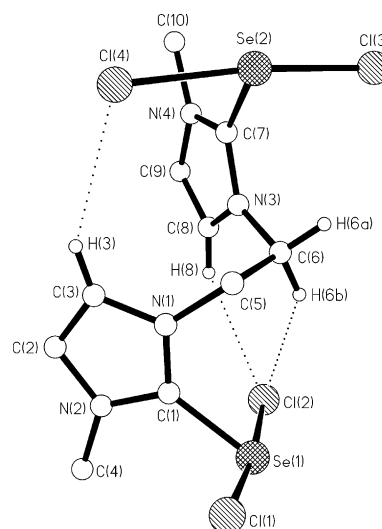


Figure 6. View of **VI** showing the numbering scheme adopted. For clarity only those hydrogen atoms involved in intramolecular hydrogen bonds (dotted lines) are shown. Bond lengths [Å] and angles [°]: C(1)–Se(1) 1.901(5), Se(1)–Cl(1) 2.3858(13), Se(1)–Cl(2) 2.5071(13), C(7)–Se(2) 1.879(5), Se(2)–Cl(3) 2.3746(16), Se(2)–Cl(4) 2.5089(15), C(1)–Se(1)–Cl(1) 88.29(14), C(1)–Se(1)–Cl(2) 86.00(14), Cl(1)–Se(1)–Cl(2) 174.20(5), C(7)–Se(2)–Cl(3) 86.22(15), C(7)–Se(2)–Cl(4) 84.84(15), Cl(3)–Se(2)–Cl(4) 171.04(5); Cl(2)···H(6b) 2.86, Cl(2)–C(6) 3.719(5), C(6)–H(6b)–Cl(2) 145; Cl(2)···H(8) 2.69, Cl(2)–C(8) 3.520(5), C(8)–H(8)–Cl(2) 146; Cl(4)···H(3) 2.93, Cl(4)–C(3) 3.766(5), C(3)–H(3)–Cl(4) 147.

fragments are asymmetric, with the longer Se–Cl distances associated with the halogen atoms involved in intramolecular hydrogen bonds, similarly to what we have already observed for **I–III** and **V** (see Figures 1, 5, 6 and the Supporting Information). Interestingly, and as already observed in other asymmetric X–E–X hypervalent systems (E = S, Se; X = Br, I),^[14b] the shorter chalcogen–halogen distances in **VI** are those associated with the halogen atoms involved in intermolecular soft–soft selenium···halogen contacts. In the case of **VI**, “T–T” pair-wise adduct associations through Se···Cl contacts lead to ladder-like supramolecular assemblies through the formation of square-planar 12–Se–4 hypervalent arrangements (Figure 7).

The black crystals, which constitute the major product of the same reaction affording **VI** (see above), were shown by crystallographic analysis to consist of co-crystallised **D2**·Cl₄ adduct units and diiodine molecules having the formulation **D2**·Cl₄·I₂ (**VII**), in good agreement with elemental analysis results. Both the hypervalent adduct and the diiodine molecules are located on crystallographic inversion centres, the Cl–Se–Cl fragments being asymmetric [Se–Cl(1) 2.3793(7), Se–Cl(2) 2.4763(7) Å]. The **D2**·Cl₄ and I₂ units interact head-to-tail through Cl···I soft–soft interactions of 3.249(1) Å involving the chlorine atom [Cl(2)] associated with the longest Se–Cl bond length in the hypervalent fragment, thus forming extended chains. These chains are coupled pair-wise by Se···Cl “clip contacts” of 3.231(1) Å at square-planar 12–Se–4 hypervalent arrangement joints (Figure 8). The resulting ribbons interact through Cl···Cl

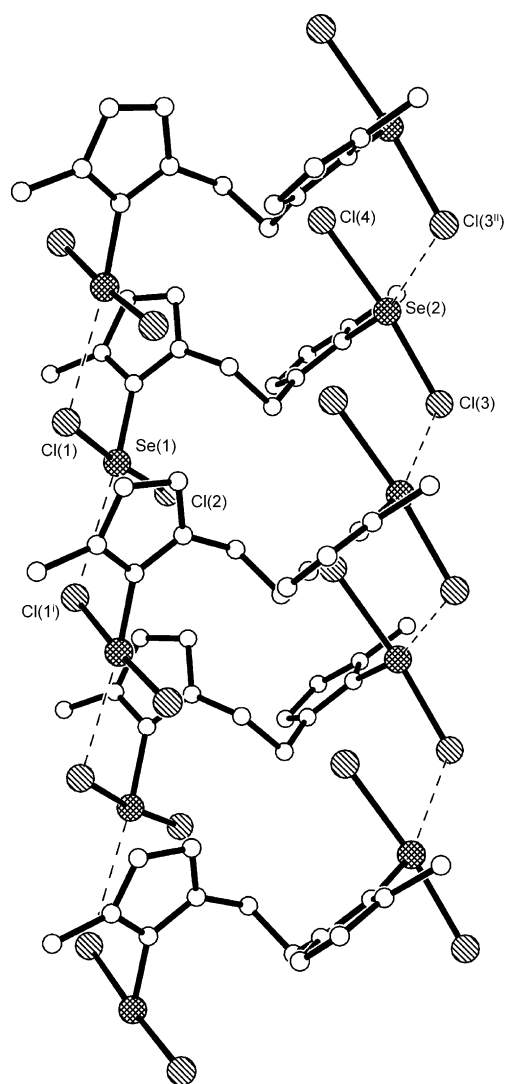


Figure 7. Partial view of the crystal packing in **VI** showing the selenium...halogen contacts (dashed lines). Bond lengths [Å] and angles [°]: Se(1)...Cl(1ⁱ) 3.259(1), Se(2)...Cl(3ⁱⁱ) 3.617(2), Cl(1)–Se(1)–Cl(1ⁱ) 88.13(3), Cl(2)–Se(1)–Cl(1ⁱ) 97.49(4), Cl(3)–Se(2)–Cl(3ⁱⁱ) 107.43(4), Cl(4)–Se(2)–Cl(3ⁱⁱ) 81.42(4). Symmetry codes: *i* = *x*, 1 – *y*, *z* – 1/2; *ii* = *x*, 1 – *y*, *z* + 1/2.

contacts of 3.465(1) Å that involve the symmetry-related chlorine atoms [Cl(1)···Cl(1ⁱⁱⁱ), *iii* = –*x*, *y*, –1/2 – *z*] associated with the shortest Se–Cl distance in the hypervalent fragments of the **D2**–Cl₄ unit to give supramolecular two-dimensional layers (Figure 8).

Interestingly, the reaction of **D2** with ICl (molar ratio of 1:2) in CH₂Cl₂ afforded compound **VIII** featuring a Cl–Se–X (X = Cl_{0.20}/I_{0.80}) moiety at one chalcogen site of the donor molecule and an X–Se–X' (X = Cl_{0.35}/I_{0.65}; X' = Cl_{0.86}/I_{0.14}) moiety at the other (Figure 9). The two hypervalent groups are approximately linear and perpendicular to the associated organic penta-atomic ring. Furthermore, the Se–X (X = Cl/I) bonds [2.5988(6)–2.6409(10) Å] are shorter than the Se–Cl distance [2.7590(11) Å], with the Se–X distance decreasing with increasing I content in the mixed occupied X positions [Se–X(3) > Se–X(4) > Se–X(1), see Figure 9] and fol-

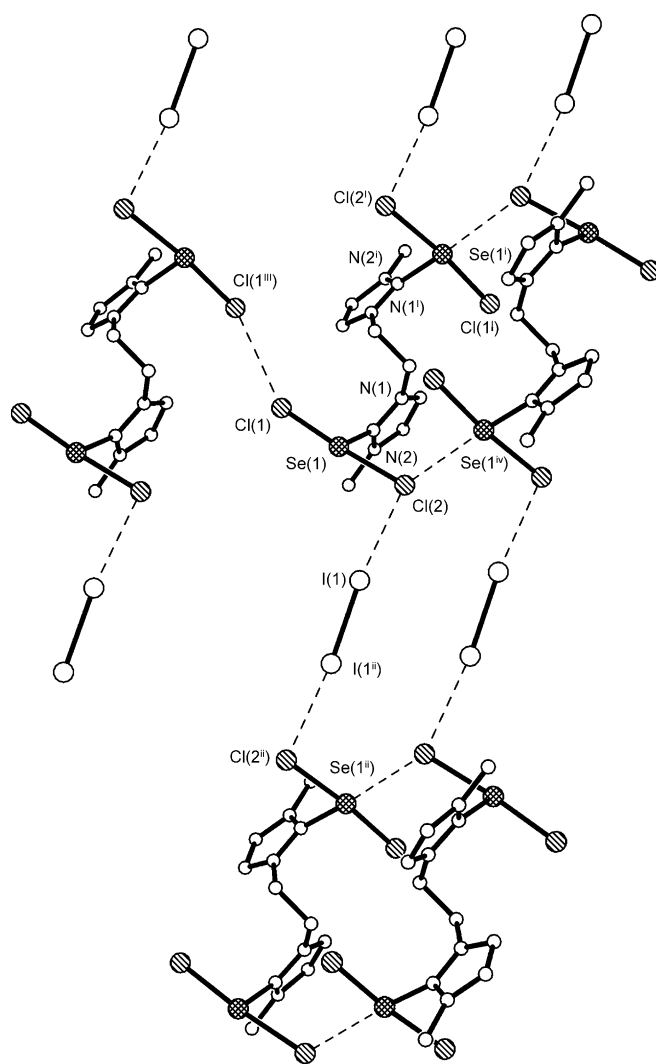


Figure 8. Partial view of the crystal packing in **VII** showing the selenium...halogen and halogen...halogen contacts (dashed lines). The numbering scheme adopted for carbon atoms is the same as in Figure 6. Bond lengths [Å] and angles [°]: C(1)–Se(1) 1.893(3), Se(1)–Cl(1) 2.3793(7), Se(1)–Cl(2) 2.4763(7), I(1)–I(1ⁱⁱ) 2.7002(4), Cl(1)···Cl(1ⁱⁱⁱ) 3.465(1), Cl(2)···I(1) 3.249(1), Cl(2)···Se(1^{iv}) 3.231(1), Se(1)–Cl(1)–Cl(1ⁱⁱⁱ) 144.06(3), Se(1)–Cl(2)–Se(1^{iv}) 119.48(3), Se(1^{iv})–Cl(2)–I(1) 135.44(2). Symmetry codes: *i* = –*x*, *y*, 1/2 – *z*; *ii* = 1 – *x*, 1 – *y*, 1 – *z*; *iii* = –*x*, *y*, –1/2 – *z*; *iv* = *x*, 1 – *y*, 1/2 + *z*.

lowing the same trend observed in **I–III** and **V**, leading to the conclusion that in 10–Se–3 Y–Se(–C<)–X (X ≠ Y = I, Br, Cl) hypervalent systems, the longer distance to the central selenium atom is that involving the most electronegative halogen site. This polarisation can also be the result of intramolecular hydrogen bonds and soft–soft selenium...halogen or halogen...halogen interactions between hypervalent moieties. In **VIII**, soft–soft X...X contacts between mixed occupied halogen sites of two symmetry-related adduct units form dimeric assemblies similar to those observed in the case of **III** (see Figure 9 and the Supporting Information). Furthermore, in **VIII**, the Cl(2)–Se–Cl(1)_{0.20}/I(1)_{0.80} moiety, on the basis of the iodine content at the disordered halogen

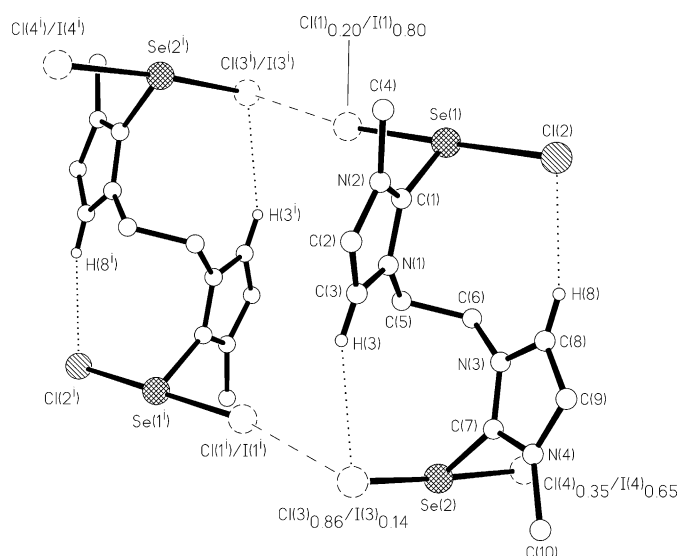


Figure 9. View of a dimeric unit of **VIII** showing the numbering scheme adopted. For clarity only those hydrogen atoms involved in intramolecular hydrogen bonds (dotted lines) are shown. Bond lengths [Å] and angles [°]: C(1)–Se(1) 1.880(4), Se(1)–X(1) 2.5988(6), Se(1)–Cl(2) 2.7590(11), C(7)–Se(2) 1.880(4), Se(2)–X(3) 2.6409(10), Se(2)–X(4) 2.6115(7), C(1)–Se(1)–X(1) 95.08(13), C(1)–Se(1)–Cl(2) 82.54(13), X(1)–Se(1)–Cl(2) 175.72(3), C(7)–Se(2)–X(3) 84.07(13), C(7)–Se(2)–X(4) 89.70(12), X(3)–Se(2)–X(4) 173.70(3); Cl(2)⋯H(8) 2.62, Cl(2)–C(8) 3.529(5), C(8)–H(8)–Cl(2) 161.2; X(3)⋯H(3) 2.82, X(3)–C(3) 3.687(5), C(3)–H(3)–X(3) 152.3; X(3)⋯X(1) 3.547(1), Se(1)–X(1)–X(3) 169.32(2) [X(1) = Cl(1)_{0.20}/I(1)_{0.80}, X(3) = Cl(3)_{0.86}/I(3)_{0.14}, X(4) = Cl(4)_{0.35}/I(4)_{0.65}]. Symmetry code: i = 1 – x, 1 – y, – z.

site, can be considered the closest ever reported to a pure Cl–Se–I 10–Se–3 hypervalent system.

FT-Raman spectroscopy: The presence of independent hypervalent adducts with Br–Se–Br or Br–Se–I moieties in crystalline **I** and **II** can be assessed by FT-Raman spectroscopy. The observed complexity of the FT-Raman spectra of these two compounds in the low frequency region reflects the disorder in their crystal structures and supports the simultaneous presence of different hypervalent systems in the solid state (see the Supporting Information). The vibrational properties of a Br–Se–Br system have been shown to resemble those of the [Br–X–Br][–] (X = I, Br) anion.^[14b,23b,26,27] In fact, as already observed for selenium hypervalent Br₂ adducts, the FT-Raman spectrum of a symmetrical Br–Se–Br group shows only a single peak near 160 cm^{–1}, as found in symmetric Br₃[–] and [Br–I–Br][–] anions. Asymmetric Br–Se–Br groups display an additional and less intense peak at around 190 cm^{–1}, as found in asymmetric Br₃[–] and [Br–I–Br][–] anions [calculated normal mode frequencies for XBr₂[–] (X = I, Br) anions in the gas phase are 89 (π_u), 156 (σ_g) and 181 (σ_u) cm^{–1} for Br₃[–] (*D*_{∞h}) and 76 (π_u), 153 (σ_g) and 163 (σ_u) cm^{–1} for IBr₂[–] (*D*_{∞h})].^[28] Similar considerations can be applied to the vibrational properties of an I–Se–Br group, which should resemble those of an [I–Br–Br][–] anion, for which normal mode stretching frequencies have been calculated at 131 and 174 cm^{–1} (I–Se–Br and [I–Br–Br][–] three-

body systems can both be described within the same MO bonding scheme (3c–4e) and show similarities in mass). Unfortunately, in **I**, **II** and **III** (the only example of a pure selenium hypervalent IBr adduct so far reported),^[17] the Se–Br distances are profoundly affected by an intramolecular hydrogen bond (see Figure 1 and the Supporting Information), thus preventing a direct structural/vibrational comparison with other selenium hypervalent Br₂ adducts or Br₃[–] and IBr₂[–] (*D*_{∞h}, *C*_{∞h}) trihalides. However, the presence in the FT-Raman spectra of **I–III** (see the Supporting Information for **II**) of peaks that roughly correspond to the expected stretching frequency modes either for the asymmetric Br₃[–] and [Br–I–Br][–] anions or for the [I–Br–Br][–] anion strongly indicates the simultaneous presence of Br–Se–Br and Br–Se–I hypervalent systems in the crystal lattices of these compounds.

Unfortunately, no vibrational spectroscopic data are available in the literature for chalcogen–hypervalent Cl₂ adducts and, therefore, no structural/vibrational comparison of the Cl–E–Cl (E = S, Se) framework with the anions [Cl–X–Cl][–] (X = I, Br) has been possible so far. The FT-Raman spectrum of compound **VI**, featuring Cl–Se–Cl moieties in which the halogen sites are fully occupied by chlorine, is dominated by a broad band centred at 267 cm^{–1}; this can be assigned to the symmetric stretching vibration mode of the hypervalent three-body system. A band at 251 cm^{–1} is also present in the FT-Raman spectrum of compound **VII**, but this is dominated by a peak at 177 cm^{–1} due to the stretching of the slightly perturbed diiodine molecule.^[26] The assignment of the band at 267 cm^{–1} in the case of **VI** and at 251 cm^{–1} in the case of **VII** is consistent with those previously reported for ICl₂[–] salts characterised by Raman peaks in the range 265–270 cm^{–1} and attributed to the symmetric stretching mode of the anion [calculated normal mode frequencies for XCl₂[–] (X = I, Br) anions in the gas phase are 109 (π_u), 218 (σ_u) and 249 (σ_g) cm^{–1} for ICl₂[–] (*D*_{∞h}) and 123 (π_u), 232 (σ_u) and 249 (σ_g) cm^{–1} for BrCl₂[–] (*D*_{∞h})].^[28] In the FT-Raman spectrum of compound **V**, therefore, the peaks at 275 (very intense), 218 and 106 cm^{–1} can be respectively attributed to the σ_g and σ_u stretchings and the π_u bending vibration modes of the Cl–Se–Cl frameworks. However, three other peaks, at 182, 131 and 75 cm^{–1}, are clearly visible in this spectrum, with the first being more intense than the second (see the Supporting Information). These peaks were tentatively assigned to the symmetric and anti-symmetric stretching and bending vibration modes, respectively, of the Cl–Se–I fragment which, according to structural data (see above), should be present in the crystal lattice as a consequence of the disorder observed at one halogen site (Figure 5). The positions of these peaks agree fairly well with the calculated normal mode frequencies of the anion [I–Br–Cl][–] [94 (π_u), 150 (σ_u) and 217 (σ_g) cm^{–1}], considering also that in **V** one Se–Cl distance in both hypervalent frameworks is remarkably affected by an intramolecular hydrogen bond (Figure 5), whereas the Se–X (X = Cl/I) moieties are involved in intermolecular selenium⋯halogen interactions, analogously to what happens in **I** and **II** for the Se–X (X =

Br/I) moieties (see Figure 2 and the Supporting Information). The same criteria can be used for the interpretation of the FT-Raman spectrum of compound **VIII**, which is dominated by two broad partially-overlapping bands centred at 190 and 174 cm^{-1} . Furthermore, the presence of peaks at around 250, 224 and 112 cm^{-1} indicates the simultaneous presence of Cl–Se–Cl, Cl–Se–I and I–Se–I hypervalent systems in the crystal lattice of **VIII**, in agreement with the structural data.

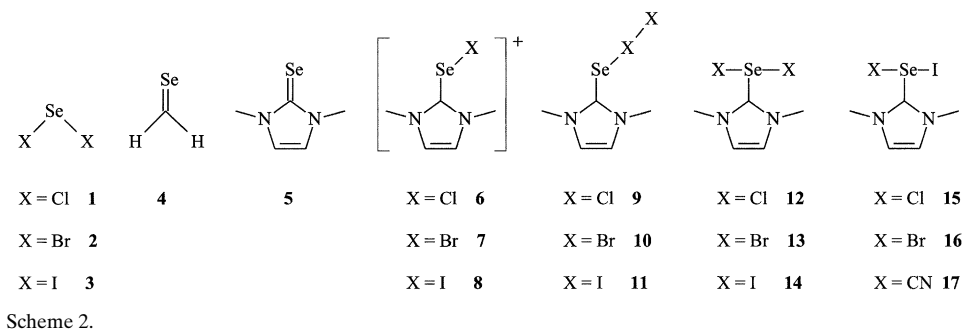
DFT calculations: Over the last few years, we have tried to provide an answer to the question of whether chalcogen compounds featuring either a linear I–Se(–C<)-X (X=Cl, Br) or a linear NC–Se(–C<)-X (X=Cl, Br, I) moiety would be better considered as strongly polarised 10–3 hypervalent compounds or $[\text{>C–Se–I}]^+\cdots\text{X}^-$ and $[\text{>C–Se–CN}]^+\cdots\text{X}^-$ ionic pairs.^[17,29] Structural and theoretical evidence tends to suggest the presence of partial covalent character in the Se–X bond and, therefore, a hypervalent nature of the central selenium atom in these asymmetric systems as compared with the symmetric X–Se(–C<)-X (X=I, Br, Cl) moieties. The linearity observed for the I–Se–X [NC–Se–X] groups so far structurally characterised could support this view, although this is not direct evidence for the hypervalency of the selenium atom. In fact, also in the case of $[\text{>C–Se–I}]^+\cdots\text{X}^-$ ionic pairs, the electrostatic interaction between the two fragments is expected to be higher along the Se–I vector. In our previous studies we observed that the widening of the >C–Se–X angle represents the most significant change in the optimised structural parameters upon lengthening one of the Se–X bonds of a symmetric X–Se–X (X=I, Br) hypervalent system leading towards the $[\text{>C–Se–X}]^+$ cation, all the other structural parameters being only slightly changed.^[14b,17,23b] In **III**, the experimental >C–Se–I angles, when compared with the calculated ones, are in agreement with a different degree of covalency and, therefore, to a different degree of hypervalency in the two I–Se–Br groups, which adopt intermediate situations between the two limiting cases, namely purely ionic $[\text{I–Se}]^+\cdots\text{Br}^-$ and covalent 3c–4e I–Se–Br.^[17]

DFT calculations so far performed on $[\text{>C–Se–X}]^+$ cations (X=I, Br, Cl) indicate a σ^* nature of the LUMO with respect to the Se–X vector and the presence of a higher positive charge on the chalcogen atom with respect to the halogen. Therefore, in terms of a CT or donor–acceptor model for the chemical bonding, the two limiting cases for a linear I–Se(–C<)-X (X=Cl, Br) moiety, covalent and ionic, would correspond, respectively, to two and zero electrons reversed from X^- into the LUMO of the cation $[\text{>C–Se–I}]^+$, all possible intermediate charge-transfer situations being conceptually possible. At the

Se–X distances found in the solid state for the I–Se(–C<)-X moieties (X=Br, Cl), a donor–acceptor interaction between the lone pair of a halide ion X^- (X=Br, Cl) and the LUMO of the cation $[\text{>C–Se–I}]^+$ would be possible and it would give a linear, highly polarised I–Se–X moiety, the amount of charge transferred from the X^- ion into the LUMO of the cation $[\text{>C–Se–I}]^+$ mainly depending on the electronegativity of the former.^[14b,17,23b] Similarly, $[\text{>C–E–CN}]^+$ cations (E=S, Se) from 1,3-dimethylimidazoline-2-chalcogenone donors are characterised by a LUMO having σ^* character with respect to the E–C–N vector and are symmetry-allowed to accept charge density from donor halides *trans*-disposed to the cyano group to give highly polarised NC–Se(–C<)-X (X=Cl, Br, I) three-body systems.^[29]

Analysis of the QTAIM properties at the BCPs of Se–C/Se–X bonds in 1–17: To better establish the degree of hypervalency of the selenium atom in chalcogen compounds featuring either a linear I–Se(–C<)-X (X=Br, Cl) or linear NC–Se(–C<)-I moiety and, therefore, the 3c–4e nature of these compounds, we performed a topological electron density analysis on model compounds **1–17** (Scheme 2) based on the quantum theory of atoms-in-molecules (QTAIM)^[30] approach developed by Bader and already applied with success to other types of hypervalent systems.^[31–35] Non-hypervalent compounds **1–5** have also been considered as reference compounds for comparing QTAIM parameters (see below). The structures of **6–17** were previously optimised at the DFT level by using the LanL2DZ basis set with effective core potentials (ECP) for halogen atoms,^[14b,17,23a] but in this work d,p polarisation functions were also added. This improved the match of the experimental Se–X bond lengths (where available) with the corresponding calculated distances, although in general these continue to be slightly overestimated. Selected experimental and optimised geometric parameters for **1–17** and the Z matrices of optimised structures have been deposited as Supporting Information.

According to QTAIM, any bonded atoms are connected by a single line, “bond path”, of locally maximum electron density, ρ , that originates a bond critical point (BCP), which represents a minimum of ρ along the bond path. The existence of a BCP between two atoms, and consequently the existence of a bond path, has been proposed as a universal indicator of bonding interactions between pairs of atoms.^[30]



The sign of the Laplacian, $\nabla^2\rho$, of the electron density at a BCP indicates two limiting situations: 1) a negative value of $\nabla^2\rho$ indicates a local charge concentration, which means that the interaction is a covalent bond, and 2) a positive value of $\nabla^2\rho$ indicates charge depletion, which means a closed-shell interaction as found in ionic bonds. It is also possible to find a positive $\nabla^2\rho$ and a relatively high ρ at the BCP, which indicates a covalent polar bond. Another important parameter is the local electronic energy density at BCP, H . The sign of H indicates whether charge accumulation at the BCP stabilises ($H < 0$) or destabilises ($H > 0$) the bonding interactions. Thus, a value of $H < 0$ indicates that the interaction shows a significant covalent contribution and, therefore, a lowering of the potential energy associated with the concentration of charge between the nuclei.^[36]

The delocalisation index, $\delta(A,B)$, is a measure of the total Fermi correlation shared between atoms A and B and indicates the extent to which electrons are delocalised over any pair of atoms and allows the determination of a bond order for the A–B bond in which such atoms are connected by a BCP.^[37] In the particular case of a formal 3c–4e bond (A–B–C), Molina-Molina and Dobado used the index $\delta(A,C)$ to determine the existence of such a hypervalent bond.^[31]

In this section, the QTAIM properties at the BCPs of all bonds involving the selenium atoms in **1–17** are analysed.

The QTAIM properties at the BCPs of the Se–C bonds in **4–17** were calculated and the main results are summarised in Table 1. The values of the calculated electron density, ρ , at the BCP range from 0.15282 to 0.19604 au, whereas the values of $\nabla^2\rho$ range from -0.05735 to 0.04616 au with H values all negative and ranging from -0.09123 to -0.15221 au.

It is important to underline the following aspects/trends of the calculated QTAIM electronic properties of the Se–C bond in **4–17**.

- 1) The nature of the Se–C bond changes on going from **4** to **5**. Bond distances, calculated charges on the atoms and QTAIM parameters are considerably different for the two compounds and the best summary parameter for this change is the value of $\delta(\text{Se,C})$, which decreases from 2.07 in **4** to 1.41 in **5**, with a change in the sign of the charge on the carbon and selenium atoms [$q(\text{C})$ and $q(\text{Se})$, respectively].
- 2) In general, the Se–C bonds in the halogen adducts show lower values of $\delta(\text{Se,C})$ than in compound **5**. Furthermore, it is possible to distinguish between the CT adducts **9–11**, with values of around 1.20, and the “T-shaped” adducts **12–17** or cation derivatives **6–8** with $\delta(\text{Se,C})$ values close to unity.
- 3) The $\nabla^2\rho$ values are negative for **4**, **6–8** and **12–17**, and positive for **5** and **9–11**. This observation is significant because the sign of $\nabla^2\rho$ at the BCP of the Se–C bond could represent an indirect criterion for classifying and distinguishing different types of compounds (in particular CT adducts from “T-shaped” hypervalent systems).
- 4) The local electronic energy density at the BCP, H , is negative in all cases, in agreement with a significant covalent character of the Se–C bond in all examples considered. Figure 10 shows the correlation between the calculated Se–C bond length and the delocalisation index, $\delta(\text{Se,C})$, for **4–17**. Accordingly, the strength of the Se–C bond in these compounds can be considered to vary from very strong (**4**) and strong (**5**) to intermediate (CT adducts), and it is typical of a single bond for “T-shaped” adducts and cations of the type [$>\text{C–Se–X}$]⁺.

The QTAIM properties at the BCPs of the Se–X bonds in **1–3** and **6–17** were also calculated and the main results are shown in Table 2. Non-hypervalent compounds **1–3** were used as references for comparison of the QTAIM parameters.

The ρ values calculated at the BCP range from 0.02760 to 0.13330 au (ρ calculated at the BCP of the Se–CN in **17**), whereas the values of $\nabla^2\rho$ range from -0.00655 to 0.07123 au, with the H values all negative and ranging from -0.00220 to -0.07093 au.

We wish to underline the following aspects/trends of the calculated QTAIM electronic properties of the Se–X bonds in **1–3** and **6–17**.

- 1) The electronic parameters (ρ , $\nabla^2\rho$, H , $\delta(\text{Se,X})$) of the Se–X bonds in non-hypervalent compounds **1–3** are very similar to those in cationic species **6–8**. The calculated $\delta(\text{Se,X})$ values for **1–3**

Table 1. QTAIM analysis of the Se–C bonds in **4–17**.

	Bond length [Å]	ρ [au]	$\nabla^2\rho$ [au]	ϵ	H [au]	$q(\text{Se})^{[a]}$	$q(\text{C})^{[a]}$	$\delta(\text{Se,C})^{[b]}$
4	1.753	0.19604	-0.05368	0.133	-0.15221	0.187 (0.151)	-0.330 (-0.519)	2.07 (2.03)
5	1.830	0.16421	0.04616	0.073	-0.10911	-0.181 (-0.264)	0.627 (0.220)	1.41 (1.37)
6	1.897	0.15453	-0.04311	0.164	-0.09294	0.565 (0.492)	0.689 (0.189)	1.08 (1.04)
7	1.898	0.15373	-0.03877	0.149	-0.09213	0.457 (0.396)	0.692 (0.196)	1.09 (1.05)
8	1.899	0.15282	-0.03340	0.130	-0.09123	0.283 (0.255)	0.692 (0.203)	1.10 (1.05)
9	1.867	0.15712	0.01142	0.088	-0.09860	0.095 (0.058)	0.690 (0.239)	1.21 (1.17)
10	1.865	0.15715	0.01676	0.068	-0.09886	0.030 (-0.018)	0.686 (0.240)	1.23 (1.18)
11	1.863	0.15719	0.02055	0.000	-0.09901	-0.055 (-0.110)	0.695 (0.248)	1.24 (1.19)
12	1.897	0.15476	-0.03625	0.215	-0.09360	0.555 (0.466)	0.758 (0.262)	1.05 (1.03)
13	1.895	0.15483	-0.03387	0.180	-0.09378	0.455 (0.357)	0.755 (0.263)	1.06 (1.03)
14	1.892	0.15492	-0.03039	0.147	-0.09406	0.310 (0.224)	0.746 (0.265)	1.07 (1.04)
15	1.893	0.15533	-0.03411	0.169	-0.09445	0.421 (0.336)	0.758(0.266)	1.05 (1.03)
16	1.893	0.15499	-0.03185	0.159	-0.09409	0.379 (0.286)	0.751 (0.264)	1.06 (1.04)
17	1.904	0.15427	-0.05735	0.163	-0.09244	0.616 (0.494)	0.750 (0.267)	1.01 (1.00)

[a] QTAIM net charge. The NPA charge [au] is shown in parentheses. [b] Delocalisation index for bonded two-centres (QTAIM). The Wiberg index (NBO) is shown in parentheses.

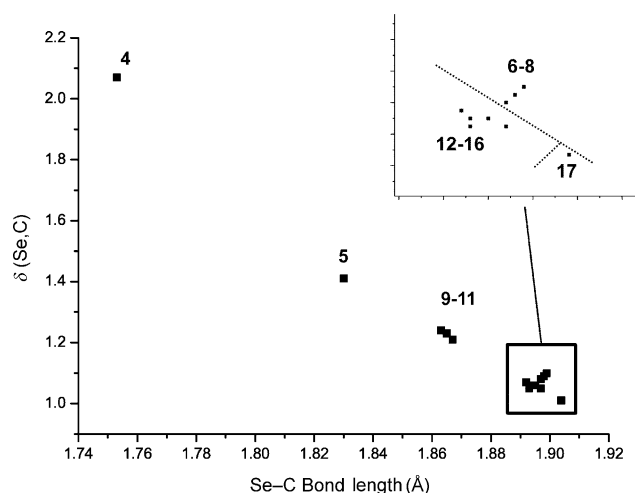


Figure 10. Calculated Se–C bond length versus delocalisation index, $\delta(\text{Se,C})$, for **4–17** (the inset shows the distribution of “T-shaped” adducts **12–17** and cations **6–8**).

Table 2. QTAIM analysis of the Se–X bonds in **1–3** and **6–17**.

Se–X	Bond length [Å]	ρ [au]	$\nabla^2\rho$ [au]	ϵ	H [au]	$q(\text{X})^{[a]}$	$\delta(\text{Se,X})^{[b]}$	$\delta(\text{X,X})^{[c]}$
1 Se–Cl	2.197	0.10836	0.04754	0.153	–0.04262	–0.270 (–0.205)	1.22 (0.98)	0.15 (0.09)
2 Se–Br	2.362	0.09380	0.00810	0.124	–0.03496	–0.169 (–0.111)	1.26 (1.01)	0.16 (0.10)
3 Se–I	2.558	0.07944	–0.00586	0.086	–0.02732	0.001 (0.034)	1.30 (1.03)	0.17 (0.11)
6 Se–Cl	2.214	0.10627	0.03543	0.136	–0.04101	–0.231 (–0.173)	1.18 (0.95)	
7 Se–Br	2.379	0.09213	0.00084	0.118	–0.03397	–0.113 (–0.074)	1.20 (0.97)	
8 Se–I	2.576	0.07754	–0.00655	0.091	–0.02647	0.083 (0.082)	1.22 (0.98)	
9 Se–Cl	2.616	0.05083	0.07123	0.073	–0.00649	–0.148 (–0.206)	0.65 (0.42)	0.26 (0.31) ^[d]
10 Se–Br	2.808	0.04163	0.05269	0.070	–0.00516	–0.095 (–0.145)	0.60 (0.37)	0.22 (0.26) ^[d]
11 Se–I	3.024	0.03439	0.04134	0.068	–0.00389	–0.031 (–0.078)	0.55 (0.31)	0.17 (0.21) ^[d]
12 Se–Cl	2.489	0.06214	0.06982	0.145	–0.01328	–0.530 (–0.507)	0.74 (0.51)	0.15 (0.18)
13 Se–Br	2.670	0.05356	0.04755	0.129	–0.01084	–0.478 (–0.453)	0.73 (0.51)	0.19 (0.24)
14 Se–I	2.886	0.04598	0.03231	0.112	–0.00846	–0.395 (–0.380)	0.74 (0.49)	0.25 (0.32)
15 Se–Cl	2.532	0.05736	0.07087	0.124	–0.01081	–0.536 (–0.518)	0.68 (0.44)	0.20 (0.24)
15 Se–I	2.842	0.04969	0.02809	0.128	–0.01030	–0.385 (–0.368)	0.80 (0.57)	
16 Se–Br	2.691	0.05141	0.04982	0.119	–0.00974	–0.488 (–0.464)	0.70 (0.46)	0.22 (0.28)
16 Se–I	2.863	0.04791	0.02977	0.121	–0.00941	–0.385 (–0.366)	0.77 (0.54)	
17 Se–CN	1.950	0.13330	0.02119	0.228	–0.07093	–0.499 (–0.399) ^[e]	0.97 (0.87) ^[f]	0.08 (0.14) ^[g]
17 Se–I	3.158	0.02760	0.03864	0.019	–0.00220	–0.631 (–0.662)	0.44 (0.23)	

[a] QTAIM net charge. The NPA charge [au] is given in parentheses. For calculated QTAIM (NPA) charges on selenium [$q(\text{Se})$] in **6–17** see Table 1; $q(\text{Se})=0.540$ (0.410) (**1**), 0.338 (0.222) (**2**), –0.001 (–0.069) (**3**). [b] Delocalisation index for bonded two-centres (QTAIM). The Wiberg index (NBO) is given in parentheses. [c] Delocalisation index for non-bonded non-adjacent two-centres (QTAIM). The equivalent Wiberg index (NBO) is given in parentheses. [d] $\delta(\text{Se,X})$. The Wiberg index (NBO) is given in parentheses. [e] QTAIM (NPA) net charge on CN [au]. [f] $\delta(\text{Se,C})$. The Wiberg index (NBO) is given in parentheses. [g] $\delta(\text{I,C})$. The Wiberg index (NBO) is given in parentheses.

and **6–8** (formally all non-hypervalent selenium compounds) range from 1.18 to 1.30, the highest values within the families of compounds considered, and typical of polar-covalent and covalent bonds.

2) CT adducts **9–11** and symmetric X–Se–X “T-shaped” adducts **12–14** (X=Cl, Br, I) are also characterised by similar QTAIM parameters for the Se–X bonds. However,

the CT adducts exhibit lower values for ρ and $\delta(\text{Se,X})$ than the corresponding symmetric “T-shaped” adducts. The reverse trend is observed for $\nabla^2\rho$ and H . In principle, it should also be possible to distinguish between CT adducts and symmetric “T-shaped” adducts on the basis of the delocalisation index $\delta(\text{Se,X})$, which is about 0.60 for the former and around 0.74 for the latter.

3) In asymmetric I–Se–X “T-shaped” adducts **15** (X=Cl) and **16** (X=Br) the calculated Se–I bond lengths are shorter and the Se–X distances longer than the corresponding bonds calculated for symmetric “T-shaped” adducts (**12–14**). This is reflected in the delocalisation index $\delta(\text{Se,X})$, which is close to about 0.80 for the Se–I bonds and to about 0.70 for the Se–X (X=Cl, Br) bonds (Table 2) in **15** and **16** as compared with the mean value of 0.74 found for symmetric “T-shaped” adducts **12–14**. In agreement with the negative value calculated for the QTAIM parameter H (Table 2), both Se–X bonds in the asymmetric I–Se–X “T-shaped” adducts have a covalent

nature with a higher polar character for the bond with the more electronegative halogen atom. Therefore these systems can be classified as 3c–4e systems, analogously to CT adducts and symmetric “T-shaped” adducts.

4) We recently elucidated the crystal structure of compound **17**, which represents a rare case of an asymmetric “T-shaped” adduct formally derived from the oxidative addition of ICN to **5**.^[29] We described the system as a strongly polarised selenium hypervalent adduct on the basis of the directionality of the I··Se–CN moiety, the value of the angle C–Se–CN, charge distribution and nature of the LUMO orbital in the cation $[\text{5-CN}]^+$. QTAIM calculations appear to confirm this view, with values of 0.97 and 0.44 for the delocalisation index and negative values of –0.07093 and –0.00220 for H calculated for the Se–CN and Se–I bonds, respectively (see Table 2).

A clear trend can be established between the QTAIM parameters calculated at the BCPs of both Se–C and Se–X bonds on passing from Cl to I in each type of compound considered. Furthermore, the observations underlined for

the delocalisation indexes $\delta(\text{Se,C})$ and $\delta(\text{Se,X})$ apply also to the calculated Wiberg indexes for the Se–C and Se–X bonds (see Tables 1 and 2), although the values of the latter indexes are slightly smaller.

Another important QTAIM parameter is the ellipticity, ϵ , at the BCP, which is a measure of the cylindricity of the charge distribution in a bond and, therefore, a measure of the π character in a bond.^[30] ϵ values close to zero indicate an axial symmetry (usually a single or triple bond) whereas higher values indicate partial π character. Calculated ϵ values at the Se–X BCP of model compounds **1–3** and **6–8** are very similar and decrease in both series on passing from Cl to Br and I. As compared with **1–3** and **6–8**, the CT adducts **9–11** are characterised by smaller ϵ values, whereas the “T-shaped” adducts **12–16** have ϵ values higher than the CT adducts and similar to those calculated for the model compounds **1–3** (Table 2). Ellipticity cannot be used to determine the hypervalent character of a bond but, in this case, it appears useful to indirectly distinguish a Se–X bond from a “T-shaped” or CT adduct. Similar conclusions can be drawn from the analysis of the ϵ values at the Se–C BCP (Table 1).

The delocalisation index $\delta(\text{X,X})$ (see Table 2) for non-bonded non-adjacent atoms has also been used previously to characterise 3c–4e systems.^[31] In our case, a slight increase is observed for this calculated parameter on passing from non-hypervalent selenium compounds **1–3** to CT and “T-shaped” adducts **9–17** (Table 2). These values for $\delta(\text{X,X})$, although quite low, do not lie close to zero, and this could already be considered an indication of a 3c–4e bond nature of the X–Se–X (X=I, Br, Cl) and I–Se–X (X=Br, Cl, CN) moieties in **12–14** and **15–17**, respectively. However, the variation in the calculated values of $\delta(\text{X,X})$ does not permit a clear distinction between genuine non-hypervalent compounds (**1–3**) and hypervalent systems. It appears that Wiberg bond indexes (see Table 2) are slightly more sensitive to the nature of the bond and could better distinguish hypervalent from non-hypervalent systems.

Therefore, we have calculated a three-centre (3c) delocalisation index $\delta(\text{A,B,C})$ for **1–17**, which should be a better indication of 3c–4e bonding in selenium hypervalent systems within the QTAIM framework. Selected values of $\delta(\text{A,B,C})$ are reported in Table 3 (see the Supporting Information for calculated $\delta(\text{A,B,C})$ indexes for **9–17**). The negative values of this index for the Se–X–X and X–Se–X (X=I, Br, Cl) moieties in **9–11** and **12–17**, respectively, indicate 3c–4e bonding.^[38a,g] For 2c–2e non-hypervalent compounds **1–3**, the much lower absolute values calculated for $\delta(\text{X,Se,X})$ clearly indicate the utility of this parameter for distinguishing between hypervalent 3c–4e compounds and 2c–2e systems. Interestingly, for CT adducts **9–11**, the index $\delta(\text{Se,X,X})$ decreases with decreasing electronegativity difference between the selenium and halogen atoms; the reverse trend is observed in the corresponding “T-shaped” adducts **12–14**. In all cases, except for **12** and **17**, the highest calculated 3c index $\delta(\text{A,B,C})$ corresponds to that in Table 3. For **12** and **17**, the highest 3c delocalisation indexes were calculated for

Table 3. Values of the three-centre delocalisation index $\delta(\text{A,B,C})$ ^[38] for selected moieties in compounds **1–3** and **9–17**.

	$\delta(\text{X,Se,X})$	$\delta(\text{Se,X,X})$	$\delta(\text{Se,C,N})$
1	–0.075		
2	–0.081		
3	–0.070		
9		–0.354	
10		–0.293	
11		–0.192	
12	–0.147		
13	–0.209		
14	–0.282		
15	–0.203		
16	–0.243		
17	–0.074 ^[a]		–0.063

[a] The reported value refers to $\delta(\text{I,Se,C})$.

the C–N–C frameworks in the penta-atomic ring, and are around –0.15. In **17**, the calculated 3c delocalisation index $\delta(\text{I,Se,C})$ is much lower than $\delta(\text{Se,X,X})$ for **9–11** and $\delta(\text{X,Se,X})$ for **12–16**. However, its negative value indicates a 3c–4e nature for this very polarised system with marked ionic character of the Se–I bond (see the Supporting Information for the $\rho(r)$ and $\nabla^2\rho(r)$ contour plots around the Cl–Se–I, Br–Se–I and I–Se–CN moieties in **15**, **16** and **17**, respectively).

Overall we can draw the same conclusions about the nature of the bonds involving the selenium atom in the compounds considered, especially those highly polarised (**15–17**), by taking into account the electron population in the natural molecular orbitals involved in the chemical bonding of the hypervalent moieties (Table 4). In particular, it is important to compare the amount of charge transferred to the anti-bonding MO (σ_{AB}^*) in the case of 2c–2e (**1–3**) and 3c–4e bonds (**9–17**) with different degrees of polarisation.

Table 4. Electron occupancies of the three valence NBOs σ_{AB} , σ_{AB}^* and n_{c} participating in the chemical bonding of the hypervalent moieties.

	A–B–C	σ_{AB}	σ_{AB}^*	n_{c}	Total ^[a]
1	Cl–Se–Cl	1.997	0.058	1.935	3.990
2	Br–Se–Br	1.997	0.059	1.934	3.990
3	I–Se–I	1.998	0.056	1.938	3.992
9	Cl–Cl–Se	1.993	0.518	1.345	3.856
10	Br–Br–Se	1.994	0.430	1.416	3.840
11	I–I–Se	1.993	0.331	1.482	3.805
12	Cl–Se–Cl	1.973	0.416	1.538	3.927
13	Br–Se–Br	1.964	0.477	1.483	3.924
14	I–Se–I	1.951	0.546	1.411	3.909
15	I–Se–Cl	1.954	0.413	1.550	3.917
16	I–Se–Br	1.953	0.468	1.494	3.915
17	NC–Se–I	1.976	0.204	1.715	3.895

[a] Total electron occupancy: $\sigma_{\text{AB}} + \sigma_{\text{AB}}^* + n_{\text{c}}$.

Topological analysis of the electron-localisation function: The topological analysis of the electron-localisation function (ELF) provides a picture of the electron-pairing regions in

the molecular space for a given distribution of nuclei and associated electron density.^[39] The ELF distributes the electron density within basins that can be classified as either core or valence basins. The core basins correspond to the core shells of electrons for each atomic species in the molecule, the valence basins correspond to the bonding and non-bonding valence electrons and are organised around and/or between core basins. Valence basins closely match the electronic domains defined by Gillespie and Hargittai in the VSEPR model.^[10]

The number of core basins, $C(A)$, connected to a given valence basin determines its synaptic order: the valence electrons shared by two interacting atoms, A and B, define a disynaptic valence basin, $V(A,B)$; the lone pairs around a given core basin $C(A)$ are denominated monosynaptic valence basins, $V(A)$. The proton is a special case because it has no core electrons.^[40] Figure 11 shows the localisation basins for molecules 1–17. Around the selenium atom in each compound considered except for 5, 9–11 and 17, two well-separated monosynaptic valence basins can be recognised (Figure 11). Compound 5 exhibits a toroidal shape for the single $V(\text{Se})$ monosynaptic basin corresponding to the two selenium lone pairs, which therefore, cannot be distinguished. Analogously, the only valence basin $V(\text{Se})$ calculated around the selenium atoms in the CT adducts 9–11 can be considered as a toroid with a section removed corresponding to the bond with the dihalogen.

Compounds 1–3 and 6–8 (2c–2e systems) have a distorted tetrahedral (disphenoidal) disposition of the $V(A)$ and

$V(A,B)$ disynaptic valence basins around the selenium atom, whereas in 12–14 (3c–4e systems), 15, 16 (polarised 3c–4e systems) and 17 (a very polarised 3c–4e system), the disposition is trigonal bipyramidal (tbp). The disposition of the valence attractors around the selenium atom in the CT adducts 9–11 (3c–4e systems) is more difficult to define due to the shape of the $V(\text{Se})$.

Test control compounds 1–3 have different forms for the valence basins $V(\text{Se},X)$ ($X=\text{Cl}, \text{Br}, \text{I}$, green in Figure 11) depending on the halogen atom. The $V(\text{Se},\text{Cl})$ in compound 1 merges with $V(\text{Cl})$. This type of topology in ELF is observed for large central atoms bound to very electronegative ligands and corresponds to bonds characterised by a marked ionic character.^[41] The $V(\text{Se},\text{Br})$ and $V(\text{Se},\text{I})$ basins in compounds 2 and 3, respectively, are situated between $C(\text{Se})$ and $C(X)$. The same situation is observed for cations 6–8. We also found that the $V(\text{I},\text{I})$ in compound 11 merges with the $C(\text{I})$ of the terminal iodine.^[41]

Topological analysis of the ELF, therefore, better reveals the distribution of the non-bonding electron-pairs around the selenium atom, which depends on the nature (2c–2e or 3c–4e) of the compound formed. The $V(\text{Se})$ in CT adducts is a half-toroid, which reveals a delocalised non-bonding electron density like that in compound 5. On the other hand, the $V(\text{Se})$ in compounds 1–3, 6–8 (2c–2e systems) and in 12–16 (3c–4e systems) shows two better-defined lobes, which clearly establishes the geometry around the selenium atom. The ELF analysis for compound 17 is quite interesting as it clearly reveals for $V(\text{Se})$ a shape intermediate between that observed for a “T-shaped” compound (12–16) and that for a pure ionic fragment (6–8).

The ELF analysis permits core basins to be distinguished from valence basins and to calculate the electron population in such basins. $N_v(\text{Se})$ represents the number of electrons in the valence shell (shared and unshared electrons) of selenium atoms of 1–17 (see the Supporting Information). This parameter could help to differentiate the hypervalent bond formation. By definition, hypervalent atoms do not obey Lewis’ octet rule and thus, for them, the number of electrons in the valence shell would be larger than 8. Examination of the $N_v(\text{Se})$ values from the ELF analysis of compounds 1–17 reveals that only compounds 1–3 and 6 would obey the octet rule. On the other hand, compounds 4, 5, 7 and 8 have $N_v(\text{Se}) > 8$, even though the selenium atoms in these compounds are involved in 2c–2e bonds and are not in a hypervalent state. According to Silvi and co-workers,^[41] this non-fulfilment of the octet rule would occur for two reasons: 1) the small difference in electronegativity between the selenium and the atoms bound to it and 2) the involvement of selenium 3d electrons.

According to our ELF analysis of 1–17, the number of electrons calculated in the core basin of the selenium atom, $C(\text{Se})$, falls between 26.5 and 27.5, and therefore below the theoretical value of 28. This means that core electrons are “migrating” to the valence basins, $V(\text{Se})$ (unshared electrons) or $V(\text{Se},X)$ (shared electrons). Therefore $N_v(\text{Se})$ does not clearly indicate when the selenium atom is in a hyperva-

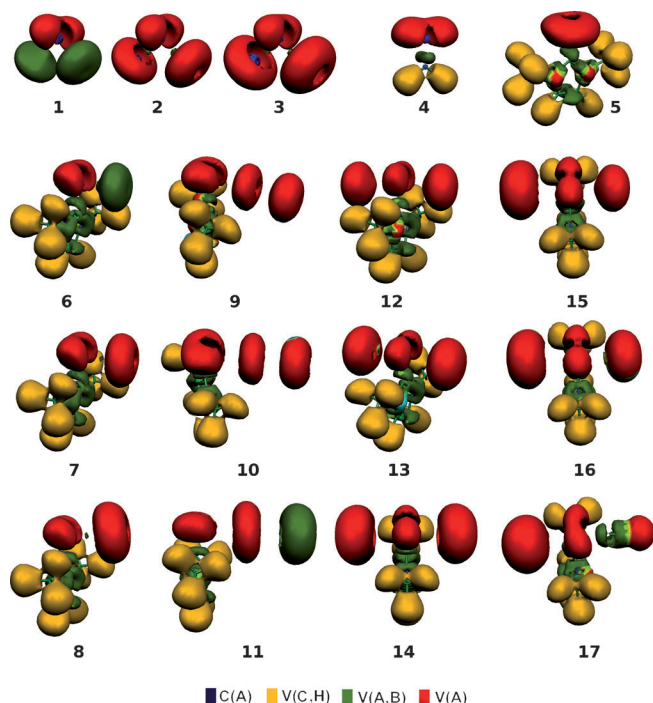


Figure 11. Electron localisation function (ELF) for 1–17 (the isosurfaces include points at which the localisation domain for the ELF is set equal to 0.7 for all molecules).

lent state and involved in a 3c–4e bond, as has already been demonstrated.^[31,41]

However, some interesting trends can be observed from the graph of $\Sigma V(\text{Se})$ versus $\Sigma V(\text{Se},\text{X})$ derived from the ELF analysis of our compounds **1–17** (Figure 12).

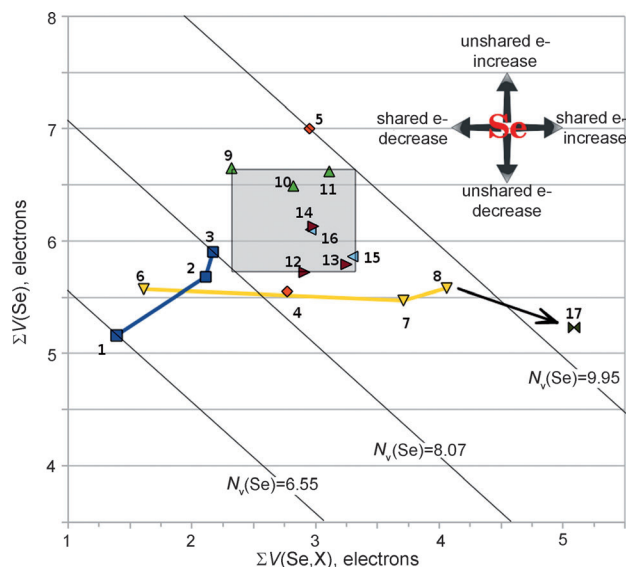


Figure 12. Distribution of the electron populations of the valence basins (see the Supporting Information) for the selenium atoms in compounds **1–17**. Diagonal lines represent the value of $N_v(\text{Se})$. The grey zone shows the limit within which the 3c–4e compounds appear.

CT and “T-shaped” adducts gather in the grey zone of the graph with $2.3 < \Sigma V(\text{Se},\text{X}) < 3.3$, $5.7 < \Sigma V(\text{Se}) < 6.6$ and $8.1 < N_v(\text{Se}) < 10.0$. Considering the series **1–3** (non-hypervalent compounds, blue line), an increase in the number of electrons in both the $V(\text{Se})$ and $V(\text{Se},\text{X})$ valence basins is observed on decreasing the electronegativity of the halogen.

Compounds **4** and **5** feature almost the same number of electrons in $V(\text{Se},\text{C})$. On the other hand, there are about 1.5 more electrons in the $V(\text{Se})$ in **5** than in **4**. These additional 1.5 electrons in the $V(\text{Se})$ of **5** could come from the imidazoline ring, but the calculated electron population of the selenium core basin (27.3 and 26.5 for **4** and **5**, respectively) clearly indicate that core electrons contribute to the population of $V(\text{Se})$ in **5**.

The series of ionic compounds **6–8** (yellow line in Figure 12) is quite different from the series **1–3**. On decreasing the electronegativity of the halogen atom only the electron population of $V(\text{Se},\text{X})$ changes by increasing from 1.6 to 4.1, whereas the population of $V(\text{Se})$ (unshared electrons) remains nearly constant.

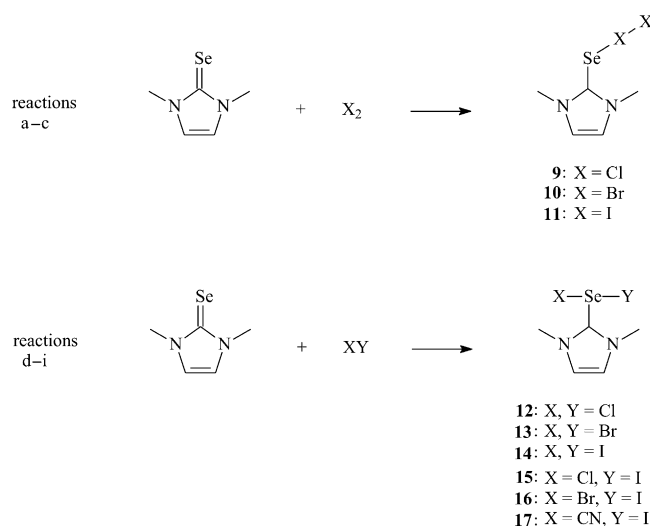
On passing from **5** to **6–8**, therefore, a decrease in the unshared electrons on the selenium atom is observed. If the halogen is more electronegative as chloride, the formation of cation **6** also produces a reduction in the shared electrons around the selenium atom. However, if the halogen is

iodine the shared valence basin $V(\text{Se},\text{X})$ increases its population.

On passing from **5** to CT (**9–11**) and “T-shaped” (**12–16**) adducts a redistribution of electrons in both valence basins $V(\text{Se})$ and $V(\text{Se},\text{X})$ is observed depending on the nature of the adduct. In particular, “T-shaped” adducts undergo a more marked reduction of the electron population in $V(\text{Se})$ compared with CT adducts. The formation of **17** causes a reduction of the electron population in the $V(\text{Se})$ of **5** to the level of that calculated for **6–8** but a remarkable increase of the population in $V(\text{Se},\text{X})$. It can be seen that CT and “T-shaped” dihalogen adducts and “T-shaped” interhalogen adducts of **5**, in terms of the electron population of the valence basins $V(\text{Se})$ and $V(\text{Se},\text{X})$, are disposed inside the triangle defined by the vertices **5–6–8** and the edges **5–9–6**, **6–7–8** and **5–11–8** (Figure 12).

Energetics of the reactions of imidazoline-2-selone donors and halogens and interhalogens:

In previous work we performed DFT calculations to gain a deeper insight into the kinetic and thermodynamic aspects of the reaction pathways that lead to the formation of CT or “T-shaped” adducts from the reactions of donor molecules containing the $>\text{C}=\text{E}$ ($\text{E}=\text{S}, \text{Se}$) group and halogens X_2 ($\text{X}=\text{Cl}, \text{Br}, \text{I}$).^[14b,23] Hypervalent “T-shaped” adducts are generally more stable than CT adducts and the formation of the $[\text{>C}-\text{E}-\text{X}]^+$ cation as an intermediate in the process leading to the different types of products was proved not to be strictly necessary because the direct interconversion of the CT into the “T-shaped” adducts is directly accessible.^[23a] As a conclusion of our analysis of the nature of the bonds in **9–17** according to QTAIM theory, we wanted to see whether thermodynamic parameters related to the formation of CT and “T-shaped” adducts could be correlated with parameters from the QTAIM analysis, in particular, the energy density at the $\text{Se}-\text{X}$ BCP. The theoretical gas-phase enthalpy changes at 298 K and 1 atm for the reactions depicted in Scheme 3 are



Scheme 3.

reported in Table 5. The “T-shaped” conformers **12–14** are more stable than the corresponding CT adducts **9–11** by 24.8, 11.3 and 1.4 kcal mol⁻¹, respectively. The energy differ-

Table 5. Theoretical gas-phase enthalpy change for the reactions depicted in Scheme 3 at 298 K and 1 atm.

Reaction	Product	ΔH_r^{298} [kcal mol ⁻¹] ^[a]
a	9	-14.3
b	10	-14.7
c	11	-13.6
d	12	-39.1
e	13	-26.0
f	14	-15.0
g	15	-23.8
h	16	-20.1
i	17	-3.2

[a] Basis set superposition error (BSSE) corrections by the counterpoise method have been applied.^[42,43]

ence between the “T-shaped” and CT adducts decreases with decreasing halogen electronegativity or increasing halogen atomic number, as has previously been reported.^[14b,23] Furthermore, the second-order perturbation analysis of the Fock matrix in the NBO basis was carried out and the $n_C \rightarrow \sigma_{AB}^*$ delocalisation interactions and stabilisation energies $\Delta E_{ij}^{(2)}$ were evaluated for **1–3** and **9–17** (see the Experimental Section). Interestingly, $\Delta E_{ij}^{(2)}$ (see the Supporting Information) significantly decreases on going from **9** to **11** (CT adducts), whereas a slight increase is observed on going from **12** to **14** (“T-shaped” adducts). Furthermore, the second-order stabilisation energies calculated for the 2c–2e systems **1–3** are much lower than those calculated for the 3c–4e systems **9–16**; in the case of **17**, $\Delta E_{ij}^{(2)}$, although much lower than the values found for **9–16**, is still about three times higher than for **1–3**. Interestingly, both theoretical ΔH_r^{298} (Table 5) and $\Delta E_{ij}^{(2)}$ (see the Supporting Information) are correlated with the energy density at the Se–X BCP (H , from the QTAIM analysis) with a discontinuity in the trends observed on passing from CT to “T-shaped” adducts (see Figure 13), which at the moment is not easy to explain (this difficulty arises mainly from the fact that the AIM properties are highly localised). However, this could represent a further way to differentiate CT from “T-shaped” adducts between donor molecules containing >C=E (E=S, Se) groups and dihalogens X₂ (X=Cl, Br, I) or interhalogens IX (X=Cl, Br).

Interestingly, a linear relationship is observed in the case of halogen and interhalogen “T-shaped” adducts between the calculated gas-phase enthalpy change, ΔH_r^{298} (reactions d–h in Scheme 3 and Table 5), and the energy density, H , at the BCP of Se–X. ΔH_r^{298} decreases (the formation reaction is more exothermic) with decreasing H (higher covalent contribution at the BCP of the Se–X bond, in the case of asymmetric “T-shaped” adducts the H value in Figure 13 is the mean of the H values calculated for each of the two Se–X bonds). The correlated decrease of both ΔH_r^{298} and H follows the increase in the electronegativity of the halogen, in

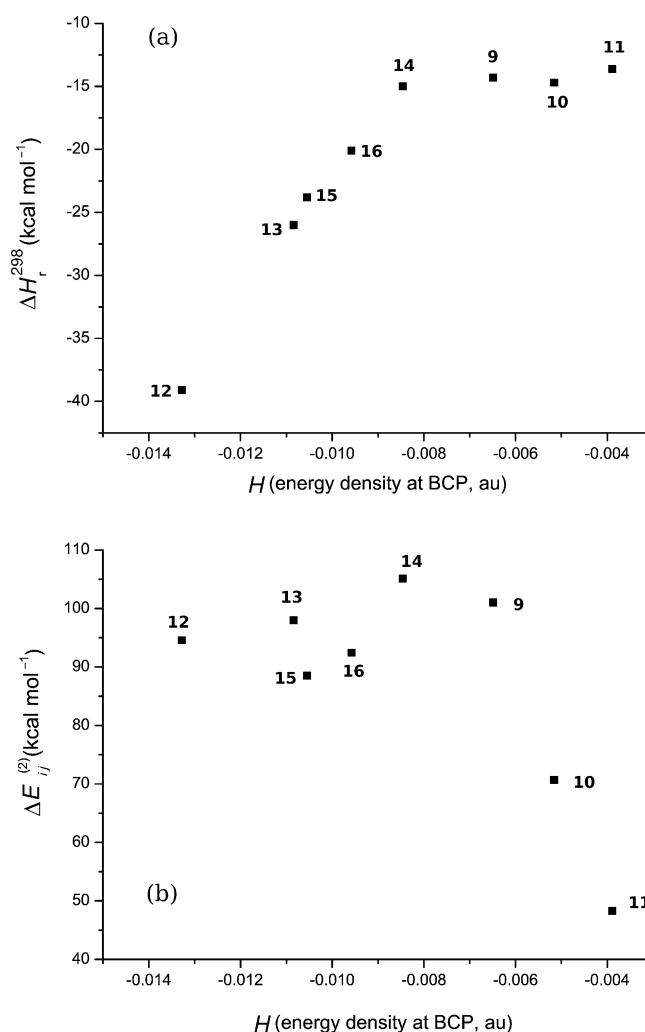


Figure 13. a) Theoretical gas-phase enthalpy change (ΔH_r^{298} , Table 5) for the formation of **9–16** (Scheme 3) and b) the second-order stabilisation energy ($\Delta E_{ij}^{(2)}$, see the Supporting Information) versus energy density at the Se–X BCP (H , from the QTAIM analysis, Table 2).

agreement with the experimental observation that “T-shaped” adducts are formed in preference to CT adducts on increasing electronegativity difference between the halogen and the chalcogen (see above). The formation of CT adducts is characterised by similar calculated ΔH_r^{298} values (–14.3 to –13.6 kcal mol⁻¹), higher than those calculated for “T-shaped” adducts, despite the H values decreasing with increasing halogen electronegativity. Presumably in this case, the formation of the Se–X bond is not determinant in defining ΔH_r^{298} , in contrast to what is expected on the basis of chemical intuition. Although the discontinuity observed in the correlation of $\Delta E_{ij}^{(2)}$ versus H is also not easy to explain, we wish to underline it because possible correlations between different experimental (or calculated) physicochemical quantities and AIM properties at BCPs are starting to attract the attention of many researchers.^[44] Interestingly, although for “T-shaped” adducts $\Delta E_{ij}^{(2)}$ does not change significantly on changing H (85–105 kcal mol⁻¹, the highest value

is for the least electronegative halogen), for CT adducts a significant linear increase in $\Delta E_{ij}^{(2)}$ is observed with decreasing H , always following the increase in the electronegativity of the halogen. Therefore the stabilisation energy associated with delocalisation from “filled” (donor) Lewis-type NBOs to “empty” (acceptor) non-Lewis NBOs ($n_X \rightarrow \sigma_{\text{Se-X}}^*$ and $n_{\text{Se}} \rightarrow \sigma_{\text{X-X}}^*$ for “T-shaped” and CT adducts, respectively) appears to be more strongly correlated in the case of CT adducts to the energy density, H , at the Se–X BCP derived from the AIM analysis, in agreement with the donor–acceptor nature of these compounds.

Conclusion

“T-Shaped” adducts featuring I–Se–X ($X = \text{Cl, Br}$) moieties are extremely rare. As part of a comprehensive study of the reactivity of the interhalogens IBr and ICl towards imidazoline-2-selone derivatives, we have isolated and fully characterised the first examples of this class of compound, which in the solid state feature interesting supramolecular arrays through chalcogen···halogen and halogen···halogen secondary bonds (soft–soft interactions). Although the adopted synthetic strategy suffers from a tendency of interhalogens IX ($X = \text{Cl, Br}$) to disproportionate, giving rise to I_2 and X_2 molecules that in turn can also undergo oxidative addition to the organic substrate, it has proved to be successful and facile approach, and it has allowed the preparation of the first examples of I–Se–X ($X = \text{Cl, Br}$) hypervalent systems. Although the structural data indicate a strong polarisation of the I–Se–X ($X = \text{Cl, Br}$) three-body systems, with Se–X distances being longer than the Se–I ones, an analysis of the QTAIM properties at the BCPs of the Se–I and Se–X bonds in model compounds in the gas phase clearly still indicates a 3c–4e bond nature for these kinds of systems with a partial degree of hypervalency for the central selenium atom. Therefore the nature of the bond in the I–Se–X ($X = \text{Cl, Br}$) moieties in the isolated compounds can be considered as intermediate between the limiting cases of purely $[\text{I-Se}]^+ \cdots \text{X}^-$ ionic couples and covalent 3c–4e I–Se–X “T-shaped” adducts. On the basis of the QTAIM theory and topological analysis of the electron localisation function (ELF), different criteria are suggested to ascertain the hypervalent nature of the selenium atoms in the compounds considered and to distinguish CT from “T-shaped” adducts, such as the three-centre delocalisation index $\delta(\text{A,B,C})$, the correlation between the stabilisation energy, $\Delta E_{ij}^{(2)}$, and the energy density at the Se–X BCP (H , from the QTAIM analysis), and the electron distribution in the valence basins around the selenium atom from the ELF analysis. In fact, the hypervalency of the central selenium atom in the X–Se–X ($X = \text{I, Br, Cl}$) and I–Se–X ($X = \text{Br, Cl}$) moieties, rather than be defined by the total number of electrons in the valence basins following the classic octet rule, could be better defined by precise limits in the electron population of the disynaptic and monosynaptic valence basins $V(\text{Se})$ and $V(\text{Se,X})$, respectively.

Experimental Section

General methods and materials: Microanalytical data were obtained by using a Fison EA CHNS-O instrument ($T = 1000^\circ\text{C}$). FT-Raman spectra, in the range $500\text{--}50\text{ cm}^{-1}$, were recorded with a resolution of 2 cm^{-1} on a Bruker RFS100 FT-Raman spectrometer fitted with an In–Ga–As detector (room temperature) operating with a Nd–YAG laser (excitation wavelength 1064 nm ; 100 mW) with a 180° scattering geometry. All reagents were purchased from Sigma–Aldrich and were Ultrapure grade. 1,1'-Methylenebis(3-methyl-4-imidazoline-2-selone) (**D1**) and 1,2-ethylenebis(3-methyl-4-imidazoline-2-selone) (**D2**) were prepared according to literature methods.^[16a]

Synthesis of D1-Br_{2,91}I_{1,09} (I), D1-Br_{3,30}I_{0,70} (II), D2-Br₂I₂ (III), [D2]²⁺(Br_{1,53}I_{1,47})[−](Br_{1,40}I_{1,60})[−] (IV), D1-Cl_{3,86}I_{0,14} (V), D2-Cl₄ (VI), D2-Cl₄I₂ (VII) and D2-Cl_{2,41}I_{1,59} (VIII): Compounds **I–VIII** were prepared from CH_2Cl_2 or CH_3CN solutions of **D1** or **D2** (0.075 mmol) and IBr in molar ratios of 1:2 or 1:4 by slow evaporation at room temperature.

D1-Br_{2,91}I_{1,09} (I): Prepared from a molar ratio of 1:2 of **D1**/IBr in CH_3CN solution, 58% yield; elemental analysis calcd (%) for $\text{C}_9\text{H}_{12}\text{Br}_{2,91}\text{I}_{1,09}\text{N}_4\text{Se}_2$: C 15.33, H 1.72, N 7.95; found: C, 15.23, H 1.69, N 7.90.

D1-Br_{3,30}I_{0,70} (II): Prepared from a molar ratio of 1:4 of **D1**/IBr in CH_3CN solution, 48% yield; elemental analysis calcd (%) for $\text{C}_9\text{H}_{12}\text{Br}_{3,30}\text{I}_{0,70}\text{N}_4\text{Se}_2$: C 15.74, H 1.76, N 8.16; found: C 15.78, H 1.79, N 8.13.

D2-Br₂I₂ (III): Prepared from a molar ratio of 1:2 of **D2**/IBr in CH_3CN solution, 33% yield; elemental analysis calcd (%) for $\text{C}_{10}\text{H}_{14}\text{Br}_2\text{I}_2\text{N}_4\text{Se}_2$: C 15.77, H 1.84, N 7.35; found: C 15.55, H 1.80, N 7.25.

[D2]²⁺(Br_{1,53}I_{1,47})[−](Br_{1,40}I_{1,60})[−] (IV): Prepared from a molar ratio of 1:4 of **D2**/IBr in CH_3CN solution, 65% yield; elemental analysis calcd (%) for $\text{C}_{10}\text{H}_{14}\text{Br}_{2,93}\text{I}_{3,07}\text{N}_4\text{Se}_2$: C 12.35, H 1.45, N 5.76; found: C 12.40, H 1.40, N 5.78.

D1-Cl_{3,86}I_{0,14} (V): Prepared from a molar ratio of 1:4 of **D1**/ICl in CH_3CN solution, 41% yield; elemental analysis calcd (%) for $\text{C}_9\text{H}_{12}\text{Cl}_{3,86}\text{I}_{0,14}\text{N}_4\text{Se}_2$: C 22.12, H 2.47, N 11.46; found: C 22.10, H 2.48, N 11.44.

D2-Cl₄ (VI) and D2-Cl₄I₂ (VII): A CH_3CN solution of **D2** and ICl (1:4 reaction molar ratio) afforded a few orange crystals of **D2-Cl₄ (VI)** and black crystals of **D2-Cl₄I₂ (VII)** in a yield of 30% after slow evaporation at room temperature.

D2-Cl₄ (VI): Elemental analysis calcd (%) for $\text{C}_{10}\text{H}_{14}\text{Cl}_4\text{N}_4\text{Se}_2$: C 24.51, H 2.88, N 11.43; found: C 24.48, H 2.86, N 11.44.

D2-Cl₄I₂ (VII): Elemental analysis calcd (%) for $\text{C}_{10}\text{H}_{14}\text{Cl}_4\text{I}_2\text{N}_4\text{Se}_2$: C 16.15, H 1.90, N 7.53; found: C 16.13, H 1.92, N 7.51.

D2-Cl_{2,41}I_{1,59} (VIII): Prepared from a molar ratio of 1:2 of **D2**/ICl in CH_2Cl_2 solution, 32% yield; elemental analysis calcd (%) for $\text{C}_{10}\text{H}_{14}\text{Cl}_{2,41}\text{I}_{1,59}\text{N}_4\text{Se}_2$: C 18.91, H 2.22, N 8.82; found: C 18.86, H 2.20, N 8.78.

Crystallography: A summary of the crystal data and refinement details for the compounds discussed in this paper are given in Table 6. Diffraction data for **D1-Br_{2,91}I_{1,09} (I)**, **D1-Br_{3,30}I_{0,70} (II)**, **D2-Br₂I₂ (III)**,^[17] **[D2]²⁺(Br_{1,53}I_{1,47})[−](Br_{1,40}I_{1,60})[−] (IV)** and **D1-Cl_{3,86}I_{0,14} (V)** were collected at 150(2) K using ω – θ scans on a Stöck Stadi-4 four-circle diffractometer equipped with an Oxford Cryosystems open-flow cryostat using graphite-monochromated $\text{MoK}\alpha$ radiation ($\lambda = 0.71073\text{ \AA}$). Diffraction data for **D2-Cl₄ (VI)**, **D2-Cl₄I₂ (VII)** and **D2-Cl_{2,41}I_{1,59} (VIII)** were collected at 150(2) K using ω scans on a Bruker SMART1000 CCD area detector diffractometer equipped with an Oxford Cryosystems open-flow cryostat using graphite-monochromated $\text{MoK}\alpha$ radiation ($\lambda = 0.71073\text{ \AA}$). Datasets were corrected for Lorentz and polarisation effects and for absorption: numerical absorption corrections by face-indexing were applied to **I–V**, whereas multi-scan corrections were applied to **VI–VIII**.^[45,46] All the structures were solved by direct methods using SHELXS97,^[47] except that of **VI**, which was solved by heavy atom methods, and completed by iterative cycles of full-matrix least-squares refinement and ΔF syntheses using SHELXL97^[48] with non-hydrogen atoms refined with anisotropic

Table 6. Summary of the crystallographic data for **I**, **II** and **IV–VIII**.^[a]

	I	II	IV	V	VI	VII	VIII
formula	C ₉ H ₁₂ Br _{2.91} I _{1.09} N ₄ Se ₂	C ₉ H ₁₂ Br _{3.30} I _{0.70} N ₄ Se ₂	C ₁₀ H ₁₄ Br _{2.93} I _{3.07} N ₄ Se ₂	C ₉ H ₁₂ Cl _{3.86} I _{0.14} N ₄ Se ₂	C ₁₀ H ₁₄ Cl ₄ N ₄ Se ₂	C ₁₀ H ₁₄ Cl ₄ I ₂ N ₄ Se ₂	C ₁₀ H ₁₄ Cl _{2.41} I _{1.59} N ₄ Se ₂
<i>M_r</i>	705.01	686.68	972.13	488.75	489.97	743.77	635.01
crystal system	triclinic	triclinic	monoclinic	triclinic	monoclinic	monoclinic	triclinic
space group	<i>P</i> 1̄ (No. 2)	<i>P</i> 1̄ (No. 2)	<i>P</i> 2/c (No. 13)	<i>P</i> 1̄ (No. 2)	<i>C</i> c (No. 9)	<i>C</i> 2/c (No. 15)	<i>P</i> 1̄ (No. 2)
<i>a</i> [Å]	7.478(5)	7.454(4)	7.734(3)	7.197(3)	20.987(3)	17.4265(11)	7.5921(6)
<i>b</i> [Å]	10.871(4)	10.876(3)	11.160(2)	10.747(4)	10.227(2)	15.1154(9)	9.7528(8)
<i>c</i> [Å]	12.264(7)	12.230(5)	12.800(2)	11.790(8)	7.8043(12)	8.1058(5)	13.2881(11)
<i>α</i> [°]	65.48(3)	65.03(3)		63.80(4)			96.870(1)
<i>β</i> [°]	79.90(6)	79.81(4)	94.71(2)	80.46(4)	90.062(2)	102.441(1)	105.774(1)
<i>γ</i> [°]	85.56(4)	85.73(3)		86.83(3)			105.637(1)
<i>V</i> [Å ³]	893.0(9)	884.6(6)	1101.1(5)	806.7(7)	1675.1(5)	2085.0(2)	891.84(13)
<i>Z</i>	2	2	2	2	4	4	2
<i>ρ</i> _{calcd} [g cm ⁻³]	2.622	2.578	2.932	2.012	1.943	2.369	2.369
<i>μ</i> (MoK _α) [mm ⁻¹]	12.527	12.846	12.977	5.481	5.047	7.020	7.270
absorption	numerical ^[45]	numerical ^[45]	numerical ^[45]	numerical ^[45]	multi-scan ^[46]	multi-scan ^[46]	multi-scan ^[46]
corrections							
min/max	0.259/0.527	0.379/0.609	0.068/0.423	0.332/0.663	0.185/0.348	0.376/0.583	0.272/0.483
transmission							
unique reflns/ <i>R</i> _{int}	3539/0.043	3462/–	2174/0.030	3172/0.057	2895/0.028	2505/0.031	4083/0.026
observed reflns	2781	2738	1795	2528	2641	2220	3653
[<i>F</i> _o ≥ 4σ(<i>F</i> _o)]							
goodness of fit	1.19	1.06	1.14	1.10	1.00	1.02	1.06
<i>R</i> ₁ / <i>wR</i> ₂ (all data)	0.0557/0.1346	0.0469/0.1414	0.0371/0.0977	0.0442/0.1150	0.0304/0.0731	0.0239/0.0611	0.0350/0.0949
largest diff. peak	1.52 to –1.77	1.17 to –1.32	1.21 to –1.67	1.11 to –0.95	0.50 to –0.60	0.83 to –1.17	1.94 to –1.40
[e Å ⁻³]							

[a] Crystallographic data for compound **III** are reported in ref. [17].

displacement parameters. Hydrogen atoms were introduced at calculated positions and refined by using a riding model, apart from those on the methyl groups of **D1** and **D2**, which were located from difference maps and refined as part of rigid groups. During the early stages of the structure refinements of **I** and **II** using a Br–Se–Br model for the two hypervalent moieties in the asymmetric unit, one of the bromine sites in both hypervalent moieties showed an anomalous displacement parameter, which suggests that these sites may be partially replaced by iodine. A competitive refinement was carried out to investigate this possibility and a final model with the following mixed-site occupancies was found to give the best fit to the data: for **I** the I/Br occupancies were 0.418(12)/0.582(12) and 0.674(12)/0.326(12) for sites 1 and 4, respectively, and for **II** 0.528(11)/0.472(11) and 0.170(11)/0.830(11) for sites 1 and 4, respectively. An analogous disorder was observed for **V** and **VIII**. In particular, for **V** only one out of four halogen sites using a Cl–Se–Cl starting model for the two independent hypervalent moieties showed an anomalous displacement parameter and following a similar treatment the occupancies were refined to 0.140(3) for I and 0.860(3) for Cl at this disordered site. For **VIII**, three out of four Cl sites were found to be disordered and this was modelled as for **V** for the independent hypervalent moieties, giving Cl/I occupancies of 0.199(3)/0.801(3), 0.860(2)/0.140(2) and 0.355(3)/0.645(3) for sites 1, 3 and 4, respectively, whereas site 2 was found to be a fully-occupied Cl. Finally, an analogous disorder was observed for one of the bromines in both counter-anions (one lying across an inversion centre) of the [**D2**]²⁺ dication in **IV**, initially refined by using a [Br–I–Br][–] model. A similar refinement led to Br[0.697(8)]/I[0.303(8)] and Br[0.531(10)]/I[0.469(10)] occupancies at the disordered sites 2 and 4, respectively. In all cases the positions and the anisotropic displacement parameters of the different halogen components at each of the disordered sites were constrained to be the same.

CCDC-816168 (**I**), 816169 (**II**), 816170 (**IV**), 816171 (**V**), 816172 (**VI**), 816173 (**VII**), and 816174 (**VIII**) contain the supplementary crystallographic data for this paper. These data can be obtained free of charge from The Cambridge Crystallographic Data Centre via www.ccdc.cam.ac.uk/data_request/cif.

Theoretical calculations: Quantum chemical calculations were performed on **1–17** (Scheme 2) and on the BrCl₂[–] (*D*_{∞h} point group) and [I–Br–Cl][–]

anions by using the commercial suite of program Gaussian 03 (Rev. E.01)^[49] at the DFT level^[50] with the hybrid B3LYP functional.^[51] Although the use of all-electron basis sets (BSs) provides better accuracy, pseudo-potential techniques are useful when relativistic effects must be taken into account. Thus, the double- ζ plus polarisation all-electron (pVDZ) BSs by Schäfer, Horn and Ahlrichs were used for carbon, hydrogen, nitrogen and selenium,^[52] whereas the LanL2DZ(dp) basis set with effective core potentials (ECP)^[53] was adopted for the halogen atoms. Vibrational analyses were used to check the nature of the stationary points and none of the optimised geometries presented imaginary frequencies at the DFT level (global minima). Theoretical gas-phase enthalpy changes for the reactions of **5** with halogens and interhalogens to give **9–17** were calculated at the same level of theory. Electronic properties for **1–17** were studied by single-point energy calculations carried out at the optimised geometries (see above) adopting 6-311++G(d,p) basis set for all atomic species but iodine, for which the 6-311G(d,p) basis set was used instead.^[54–56] This procedure was adopted to prevent the failure of the topological analysis of the coreless electron densities obtained from a pseudo-potential calculation.^[55a]

The QTAIM^[30] study on **1–17** was performed by using AIMAll,^[57a] AIM2000^[57b] and XAIM.^[57c] NPA charges, Wiberg indexes and second-order analysis of the Fock matrix energies were calculated by using NBO Version 3.1.^[58] The analysis of the ELF function was carried out with TopMod^[59,60] and the ELF isosurfaces were visualised with Molekel.^[61] $\delta(A,B)$ values were determined from AIMAll calculations whereas $\delta(A,B,C)$ values were obtained from GaussPop as a Mulliken-like three-centre bond index (RHF/6-311G(d,p) for all atoms).^[38] The second-order perturbation analysis of the Fock matrix in the NBO basis^[58] was also carried out and the $n_C \rightarrow \sigma^*_{AB}$ delocalisation interactions in compounds **1–3** and **9–17** were examined. The stabilisation energy, $\Delta E_{ij}^{(2)}$, due to electron delocalisation from the donor NBO (*i*) to the acceptor NBO (*j*) was estimated to be $\Delta E_{ij}^{(2)} = q_i [F(i,j)^2] / (\lambda_i - \lambda_j)$, in which q_i is the donor orbital occupancy, λ_i and λ_j are the diagonal elements (orbital energies) and $F(i,j)$ is the off-diagonal NBO Fock matrix element.

Acknowledgements

This work was supported by the Università degli Studi di Cagliari, the Generalitat de Catalunya (2009/SGR/0027) and the Spanish Ministerio de Ciencia e Innovación (CTQ2010-16237). Access to the computational facilities of the Centre de Supercomputació de Catalunya (CESCA) and the CSIC Computing Centre (CTI) is also gratefully acknowledged. E.J.J.-P. thanks Pablo Vitoria for help in obtaining the ELF 3D graphs with coloured basins according to their type, Gonzalo Millán for Fortran compilation and Prof. Ponec for providing GaussPop software. We also thank the EPSRC (UK) for the provision of X-ray diffractometers.

- [1] a) K. J. Wynne in *Sulfur Research Trends, Advances in Chemistry Series 110* (Eds.: D. J. Miller, T. Wiewiorowski), American Chemical Society, Washington, **1972**, pp. 150–161; b) Z. Xu in *Handbook of Chalcogen Chemistry: New Perspective in Sulfur, Selenium and Tellurium* (Ed.: F. A. Devillanova), RSC Publishing, Cambridge, UK, **2007**, Chapter 8.1, pp. 457–476.
- [2] B. Krebs, F.-P. Ahlers, *Adv. Inorg. Chem.* **1990**, *35*, 235–317.
- [3] K. J. Wynne, P. S. Pearson, M. G. Newton, J. Golen, *Inorg. Chem.* **1972**, *11*, 1192–1196.
- [4] D. J. Williams, K. J. Wynne, *Inorg. Chem.* **1976**, *15*, 1449–1451.
- [5] A. J. Arduengo, E. M. Burgess, *J. Am. Chem. Soc.* **1977**, *99*, 2376–2378.
- [6] a) D. J. Williams, D. Vanderver, B. R. Crouse, R. R. Raye, T. Carter, K. S. Hagen, M. Brewer, *Main Group Chem.* **1997**, *2*, 61–66; b) F. Bigoli, P. Deplano, F. A. Devillanova, V. Lippolis, M. L. Mercuri, M. A. Pellinghelli, E. F. Trogu, *Eur. J. Inorg. Chem.* **1998**, 137–141.
- [7] C. W. Perkins, J. C. Martin, A. J. Arduengo, W. Lau, A. Alegrie, *J. K. Kocki, J. Am. Chem. Soc.* **1980**, *102*, 7753–7759.
- [8] N. Khun, A. Al-Sheikh, *Coord. Chem. Rev.* **2005**, *249*, 829–857.
- [9] a) A. J. Arduengo III, H. V. Rasika Dias, R. L. Harlow, M. Kline, *J. Am. Chem. Soc.* **1992**, *114*, 5530–5534; b) A. J. Arduengo, H. V. Rasika Dias, J. C. Calabrese, *Chem. Lett.* **1997**, 143–144.
- [10] R. J. Gillespie, I. Hargittai, *The VSEPR Model of Molecular Geometry*, Allyn and Bacon, Boston, Massachusetts, USA, **1991**.
- [11] *Chemistry of Hypervalent Compounds* (Ed.: K.-Y. Akiba), Wiley-VCH, New York, **1999**.
- [12] The notation 10-E-3 ($R_2C=E$ donors) or 10-E-4 (R_2E donors) for X–E(R)–X “T-shaped” hypervalent adducts (R = organic framework) proposed by Arduengo and co-workers^[7] identifies these compounds concisely, considering that the term hypervalent does not necessarily require the involvement of a d orbital from the central E atom to explain the bond nature of the bonding in the X–E(R)–X system.^[11]
- [13] M. C. Aragoni, M. Arca, F. A. Devillanova, A. Garau, F. Isaia, V. Lippolis, A. Mancini, *Bioinorg. Chem. Appl.* **2007**, 17416.
- [14] a) N. Bricklebank, P. J. Skabara, D. E. Hibbs, M. B. Hursthouse, K. M. A. Malik, *J. Chem. Soc., Dalton Trans.* **1999**, 3007–3014; b) M. C. Aragoni, M. Arca, F. Demartin, F. A. Devillanova, A. Garau, F. Isaia, F. Lelj, V. Lippolis, G. Verani, *Chem. Eur. J.* **2001**, *7*, 3122–3133.
- [15] a) F. A. Devillanova, G. Verani, F. Demartin, M. Arca, A. Garau, V. Lippolis, F. Isaia, M. C. Aragoni, *Trends Inorg. Chem.* **1999**, *6*, 1–18; b) P. D. Boyle, S. M. Godfrey, *Coord. Chem. Rev.* **2001**, *223*, 265–299.
- [16] a) F. Bigoli, A. M. Pellinghelli, P. Deplano, F. A. Devillanova, V. Lippolis, M. L. Mercuri, E. F. Trogu, *Gazz. Chim. It.* **1994**, *124*, 445–454; b) N. Kuhn, T. Kratz, G. Henkel, *Chem. Ber.* **1994**, *127*, 849–851; c) N. Kuhn, R. Fawzi, T. Kratz, M. Steimann, G. Henkel, *Phosphorus Sulfur Silicon Relat. Elem.* **1996**, *112*, 225–233.
- [17] M. C. Aragoni, M. Arca, A. J. Blake, F. A. Devillanova, W.-W. du Mont, A. Garau, F. Isaia, V. Lippolis, G. Verani, C. Wilson, *Angew. Chem.* **2001**, *113*, 4359–4362; *Angew. Chem. Int. Ed.* **2001**, *40*, 4229–4232.
- [18] C. Ouvrard, J.-Y. Le Questel, M. Berthelot, C. Laurence, *Acta Crystallogr. Sect. B* **2003**, *59*, 512–526.
- [19] a) G. J. Corban, S. K. Hadjikakou, N. Hadjiliadis, M. Kubicki, E. R. T. Tiekink, I. S. Butler, E. Drougas, A. M. Kosmas, *Inorg. Chem.* **2005**, *44*, 8617–8627; b) V. Daga, S. K. Hadjikakou, N. Hadjiliadis, M. Kubicki, J. H. Z. Santos, I. S. Butler, *Eur. J. Inorg. Chem.* **2002**, 1718–1728; c) C. D. Antoniadis, G. J. Corban, S. K. Hadjikakou, N. Hadjiliadis, M. Kubicki, S. Warner, I. S. Butler, *Eur. J. Inorg. Chem.* **2003**, 1635–1640; d) C. D. Antoniadis, S. K. Hadjikakou, N. Hadjiliadis, M. Kubicki, I. S. Butler, *Eur. J. Inorg. Chem.* **2004**, 4324–4329.
- [20] a) F. Bigoli, F. Demartin, P. Deplano, F. A. Devillanova, F. Isaia, V. Lippolis, M. L. Mercuri, M. A. Pellinghelli, E. F. Trogu, *Inorg. Chem.* **1996**, *35*, 3194–3201; b) M. C. Aragoni, M. Arca, F. Demartin, F. A. Devillanova, A. Garau, F. Isaia, V. Lippolis, G. Verani, *J. Am. Chem. Soc.* **2002**, *124*, 4538–4539.
- [21] P. D. Boyle, W. I. Cross, S. M. Godfrey, C. A. McAuliffe, R. G. Prichard, S. Teat, *J. Chem. Soc. Dalton Trans.* **1999**, 2219–2224.
- [22] M. D. Rudd, S. V. Linderman, S. Husebye, *Acta Chem. Scand.* **1997**, *51*, 689–708.
- [23] a) M. C. Aragoni, M. Arca, F. A. Devillanova, P. Grimaldi, F. Isaia, F. Lelj, V. Lippolis, *Eur. J. Inorg. Chem.* **2006**, 2166–2174; b) M. C. Aragoni, M. Arca, F. Demartin, F. A. Devillanova, A. Garau, F. Isaia, V. Lippolis, G. Verani, *Dalton Trans.* **2005**, 2252–2258.
- [24] W.-W. du Mont, C. G. Hrib in *Handbook of Chalcogen Chemistry: New Perspectives in Sulfur, Selenium and Tellurium* (Ed.: F. A. Devillanova), RSC, Cambridge, **2007**, Chapter 13, pp. 833–872.
- [25] a) F. Cristiani, F. Demartin, F. A. Devillanova, F. Isaia, V. Lippolis, G. Verani, *Inorg. Chem.* **1994**, *33*, 6315–6324; b) N. Bricklebank, S. M. Godfrey, C. A. McAuliffe, R. G. Prichard, *J. Chem. Soc. Dalton Trans.* **1993**, 2261–2266; c) N. N. Greenwood, A. Earnshaw, *Chemistry of the Elements*, Pergamon, New York, **1984**.
- [26] M. Arca, M. C. Aragoni, F. A. Devillanova, A. Garau, F. Isaia, V. Lippolis, A. Mancini, G. Verani, *Bioinorg. Chem. Appl.* **2006**, 58937.
- [27] a) C. G. Hrib, F. Ruthe, E. Seppälä, M. Bätcher, C. Druckenbrodt, C. Wismach, P. G. Jones, W.-W. du Mont, V. Lippolis, F. A. Devillanova, M. Bühl, *Eur. J. Inorg. Chem.* **2006**, 88–100; b) C. G. Hrib, P. G. Jones, W.-W. du Mont, V. Lippolis, F. A. Devillanova, *Eur. J. Inorg. Chem.* **2006**, 1294–1302.
- [28] M. C. Aragoni, M. Arca, F. A. Devillanova, M. B. Hursthouse, S. L. Huth, F. Isaia, V. Lippolis, A. Mancini, H. R. Ogilvie, G. Verani, *J. Organomet. Chem.* **2005**, *690*, 1923–1934.
- [29] M. C. Aragoni, M. Arca, F. Demartin, F. A. Devillanova, A. Garau, P. Grimaldi, F. Lelj, V. Lippolis, G. Verani, *Eur. J. Inorg. Chem.* **2004**, 2363–2368.
- [30] a) R. Bader, *Atoms in Molecules: A Quantum Theory*, Clarendon Press, Oxford, **1994**; b) C. F. Matta, R. J. Boyd, *The quantum theory of atoms-in-molecules*, Wiley-VCH, Weinheim, **2007**.
- [31] J. Molina-Molina, J. A. Dobado, *Theor. Chem. Acc.* **2001**, *105*, 328–337.
- [32] D. Barton, M. Hall, Z. Lin, S. Parekh, J. Reibenspies, *J. Am. Chem. Soc.* **1993**, *115*, 5056–5059.
- [33] J. A. Dobado, H. Martínez-García, J. Molina-Molina, *Inorg. Chem.* **1999**, *38*, 6257–6260.
- [34] J. A. Dobado, H. Martínez-García, J. Molina-Molina, M. R. Sundberg, *J. Am. Chem. Soc.* **2000**, *122*, 1144–1149.
- [35] W. Nakanishi, T. Nakamoto, S. Hayashi, T. Sasamori, N. Tokitoh, *Chem. Eur. J.* **2007**, *13*, 255–268.
- [36] D. Cremer, E. Kraka, *Angew. Chem.* **1984**, *96*, 612–614; *Angew. Chem. Int. Ed. Engl.* **1984**, *23*, 627–628.
- [37] a) J. G. Ángyán, M. Loos, I. Mayer, *J. Phys. Chem.* **1994**, *98*, 5244–5248; b) X. Fradera, J. Poater, S. Simon, M. Duran, M. Solà, *Theor. Chem. Acc.* **2002**, *108*, 214–224.
- [38] a) R. Ponec, I. Mayer, *J. Phys. Chem. A* **1997**, *101*, 1738–1741; b) R. Ponec, A. Duben, *J. Comput. Chem.* **1999**, *20*, 760–771; c) R. Bochicchio, R. Ponec, A. Torre, L. Lain, *Theor. Chem. Acc.* **2001**, *105*, 292–298; d) R. Ponec, J. Roithová, X. Gironés, K. Jug, *J. Mol. Struct.: THEOCHEM* **2001**, *545*, 255–264; e) A. Torre, L. Lain, R. Bochicchio, R. Ponec, *J. Math. Chem.* **2002**, *32*, 241–248; f) R. Ponec, D. Cooper, *Int. J. Quantum Chem.* **2004**, *97*, 1002–1011; g) T. Kar, E. S. Marcos, *Chem. Phys. Lett.* **1992**, *192*, 14–20.

- [39] a) A. D. Becke, K. E. Edgecombe, *J. Chem. Phys.* **1990**, *92*, 5397–5403; b) B. Silvi, A. Savin, *Nature* **1994**, *371*, 683–686.
- [40] B. Silvi, *J. Mol. Struct.* **2002**, *614*, 3–10.
- [41] S. Noury, B. Silvi, R. Gillespie, *Inorg. Chem.* **2002**, *41*, 2164–2172.
- [42] S. F. Boys, F. Bernardi, *Mol. Phys.* **1970**, *19*, 553–556.
- [43] F. B. van Duijneveldt, J. G. C. M. van Duijneveldt-van de Rijdt, J. H. van Lenthe, *Chem. Rev.* **1994**, *94*, 1873–1885.
- [44] I. S. Bushmarinov, K. A. Lyssenko, M. Yu Antipin, *Russ. Chem. Rev.* **2009**, *78*, 283–302.
- [45] X-RED. Program for data reduction and absorption correction. Stoë and Cie, Darmstadt, Germany, **1997**.
- [46] G. M. Sheldrick, SADABS Area-Detector Absorption Correction Program; Bruker AXS Inc.: Madison, WI, **1996–2008**.
- [47] SHELXS86 and SHELXS97, G. M. Sheldrick, *Acta Crystallogr. Sect. A* **1990**, *46*, 467–473.
- [48] SHELXL97, G. M. Sheldrick, *Acta Crystallogr. Sect. A* **2008**, *64*, 112–122.
- [49] Gaussian 03, Revision E.01, M. J. Frisch, G. W. Trucks, H. B. Schlegel, G. E. Scuseria, M. A. Robb, J. R. Cheeseman, J. A. Montgomery, Jr., T. Vreven, K. N. Kudin, J. C. Burant, J. M. Millam, S. S. Iyengar, J. Tomasi, V. Barone, B. Mennucci, M. Cossi, G. Scalmani, N. Rega, G. A. Petersson, H. Nakatsuji, M. Hada, M. Ehara, K. Toyota, R. Fukuda, J. Hasegawa, M. Ishida, T. Nakajima, Y. Honda, O. Kitao, H. Nakai, M. Klene, X. Li, J. E. Knox, H. P. Hratchian, J. B. Cross, V. Bakken, C. Adamo, J. Jaramillo, R. Gomperts, R. E. Stratmann, O. Yazyev, A. J. Austin, R. Cammi, C. Pomelli, J. W. Ochterski, P. Y. Ayala, K. Morokuma, G. A. Voth, P. Salvador, J. J. Dannenberg, V. G. Zakrzewski, S. Dapprich, A. D. Daniels, M. C. Strain, O. Farkas, D. K. Malick, A. D. Rabuck, K. Raghavachari, J. B. Foresman, J. V. Ortiz, Q. Cui, A. G. Baboul, S. Clifford, J. Cioslowski, B. B. Stefanov, G. Liu, A. Liashenko, P. Piskorz, I. Komaromi, R. L. Martin, D. J. Fox, T. Keith, M. A. Al-Laham, C. Y. Peng, A. Nanayakkara, M. Challacombe, P. M. W. Gill, B. Johnson, W. Chen, M. W. Wong, C. Gonzalez, J. A. Pople, Gaussian, Inc., Wallingford CT, **2004**.
- [50] a) R. G. Parr, W. Yang, *Density-Functional Theory of Atoms and Molecules*, Oxford University Press, Oxford, **1989**; b) E. S. Kryachko, E. V. Ledeña, *Energy Density Functional Theory of Many-Electron Systems*, Kluwer Academic, Dordrecht, **1990**.
- [51] C. Lee, W. Yang, R. G. Parr, *Phys. Rev. B* **1988**, *37*, 785–789.
- [52] A. Schäfer, H. Horn, R. Ahlrichs, *J. Chem. Phys.* **1992**, *97*, 2571–2577.
- [53] a) P. J. Hay, W. R. Wadt, *J. Chem. Phys.* **1985**, *82*, 270–283; b) W. R. Wadt, P. J. Hay, *J. Chem. Phys.* **1985**, *82*, 284–298; c) W. R. Wadt, P. J. Hay, *J. Chem. Phys.* **1985**, *82*, 299–310; d) C. E. Check, T. O. Faust, J. M. Bailey, B. J. Wright, T. M. Gilbert, L. S. Sunderlin, *J. Phys. Chem. A* **2001**, *105*, 8111–8116.
- [54] M. N. Glukhovtsev, A. Pross, M. P. McGrath, L. Radom, *J. Chem. Phys.* **1995**, *103*, 1878–1885.
- [55] a) D. Feller, *J. Comput. Chem.* **1996**, *17*, 1571–1586; b) K. Schuchardt, B. Didier, T. Elsethagen, L. Sun, V. Gurumoorthi, J. Chase, J. Li, T. Windus, *J. Chem. Inf. Model.* **2007**, *47*, 1045–1052; c) S. F. Vyboishchikov, A. Sierraalta, G. Frenking, *J. Comput. Chem.* **1997**, *18*, 416–429.
- [56] Basis sets were obtained from the Basis Set Exchange (BSE) Library v.1.2.2.
- [57] a) T. A. Keith, AIMAll (Version 09.02.01, aim.tkgristmill.com) **2008**; b) F. Biegler-König, AIM2000, University of Applied Sciences, Bielefeld, Germany; c) J. C. Ortiz, C. Bo, XAIM-1.0 1998.
- [58] a) E. D.; Glendening, A. E. Reed, J. E. Carpenter, F. Weinhold, NBO Version 3.1; b) F. Weinhold, C. Landis, Valency and bonding: a natural bond orbital donor–acceptor perspective; Cambridge University Press, Cambridge, UK, **2005**.
- [59] S. Noury, X. Krokidis, F. Fuster, B. Silvi, TopMod package, Laboratoire de Chimie Théorique, Université Pierre et Marie Curie, Paris, 1997, available at <http://www.lct.jussieu.fr/silvi>.
- [60] S. Noury, X. Krokidis, F. Fuster, B. Silvi, *Comput. Chem. Eng.* **1999**, *23*, 597–604.
- [61] S. Portmann, Molekel, Version 4.3. linux, 11. Nov. 2002.

Received: March 29, 2011
Published online: August 25, 2011